Chapter 1 Introduction

1.1 Need for Fiber Optic Communications

The advent of telegraphy in the 1830s began the era of electrical communications. The bit rate could be increased to ~10b/s by the use of new coding techniques, such as Morse code. The use of intermediate relay stations allowed communication over long distances (~1000km). The first successful transatlantic telegraph cable went into operation in 1866. The invention of the telephone in 1876 brought a major change in as much as electric signals were transmitted in analog form through a continuously varying electric current. Analog electrical techniques were to dominate communication systems for about one century.

The development of worldwide telephone networks during the twentieth century led to many advances in the design of electrical communication systems. The use of coaxial cables in replacement of wire pairs increased system capacity considerably. The first coaxial-cable system, put into service in 1940, was a 3-MHz system capable of transmitting 300 voice channels or a single television channel. The bandwidth of such systems is limited by the frequency-dependent cable losses, which increase rapidly for frequencies beyond 10MHz. This limitation led to the development of microwave communication systems in which an electromagnetic carrier wave with frequencies of ~1 to 10GHz is used to transmit signals. The first actual operation of microwave communications at the carrier frequency of 4GHz was put into service in 1948. Since then, both coaxial and microwave systems have evolved considerably and are able to operate at bit rates of ~100Mb/s. The most advanced coaxial system, of such a high-speed coaxial system is the small repeater spacing (~1km), which makes the system relatively expensive to operate. Microwave communication systems generally allow a larger repeater spacing, but their bit rate is also limited by the carrier frequency of such

waves. A commonly used figure of merit for communication systems is the big rate-distance product, BL, where B is the bit rate and L is the repeater spacing. Figure 1.1 shows how the BL product has increased through technological advances during the last century and a half.

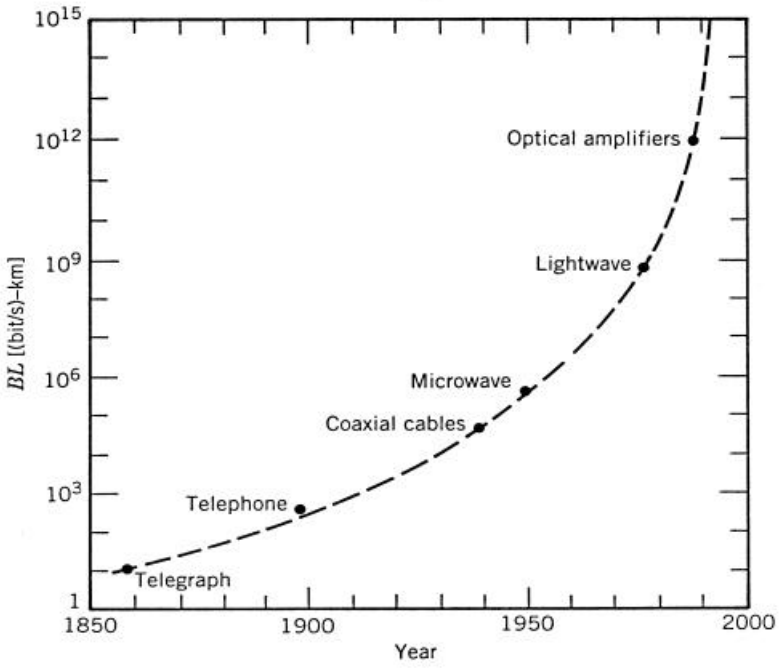

Figure 1.1 Increase in bit rate-distance product BL during the period 1850-2000

Communication systems with BL~100 (Mb/s)-km were available by 1970 and were limited to such values because of fundamental limitations.

It was realized during the second half of the twentieth century that an increase of several orders of magnitude in the BL product would be possible if optical waves were used as the carrier. However, neither a coherent optical source nor a suitable transmission medium was available during the 1950s. The invention of the laser and its demonstration in 1960 solved the first problem. Attention was then focused on finding ways for using laser light for optical communications. It was suggested in 1966 that optical fibers might be the best choice, as they are capable of guiding the light in a manner similar to the guiding of electrons in copper wires. The main problem was the

high loss of optical fibers—fibers available during the 1960s had losses in excess of 1000dB/km. A breakthrough occurred in 1970 when the fiber loss could be reduced to about 20dB/km in the wavelength region near 1ìm. At about the same time, GaAs semiconductor lasers, operating continuously at room temperature, were demonstrated. The simultaneous availability of a compact optical source and a low-loss optical fiber led to a worldwide effort for developing fiber-optic communication systems. Figure 1.2 shows the progress in the performance of light wave systems realized after 1974 through several generations of development.

The block diagram of the fiber-optical communication system is illustrated in Figure 1.3.

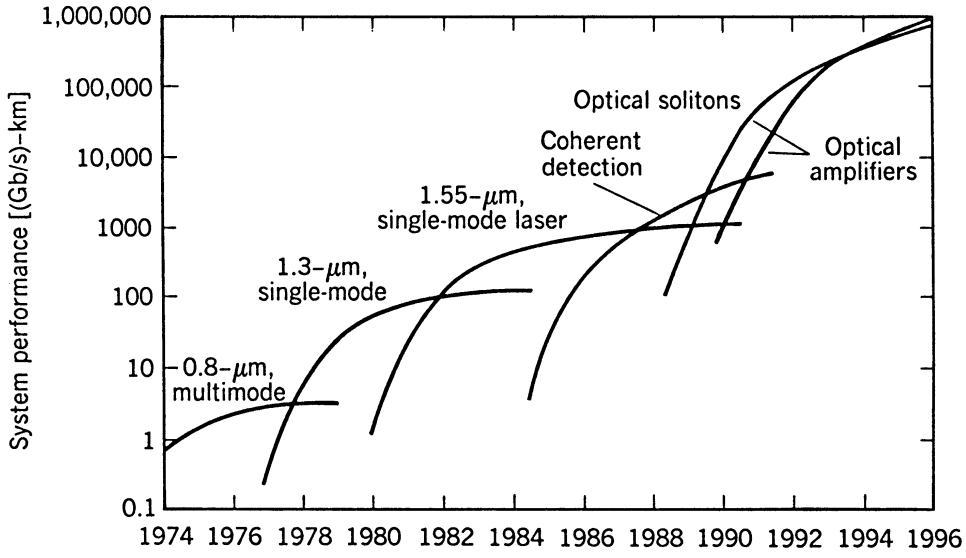

Figure 1.2 Progress in lightwave communication technology over the period 1974-1996

OPTICAL COMMUNICATION SYSTEMS

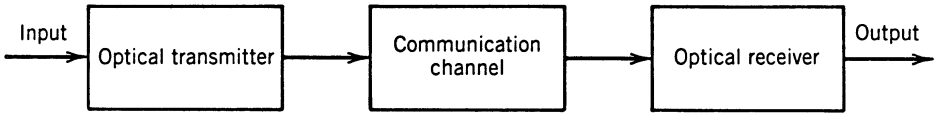

Figure 1.3 Generic optical communication system

1.2 WDM Lightwave Systems

Wavelength division multiplexing (WDM) corresponds to the scheme in which multiple optical carriers at different wavelengths are modulated by using independent electrical bit streams and are then transmitted over the same fiber. The optical signal at the receiver is demultiplexed into separate channels by their wavelengths. WDM has the potential for exploiting the large bandwidth offered by the optical fiber. For example, hundreds of 10Gb/s channels can be transmitted over the same fiber if the channel spacing is reduced to 40-50 GHz. Figure 1.4 shows the low-loss transmission windows of optical fibers centered near 1.3 and 1.55ìm. Each window covers a bandwidth of more than 10 THz, indicating that the total capacity of WDM systems may exceed 10 Tb/s.

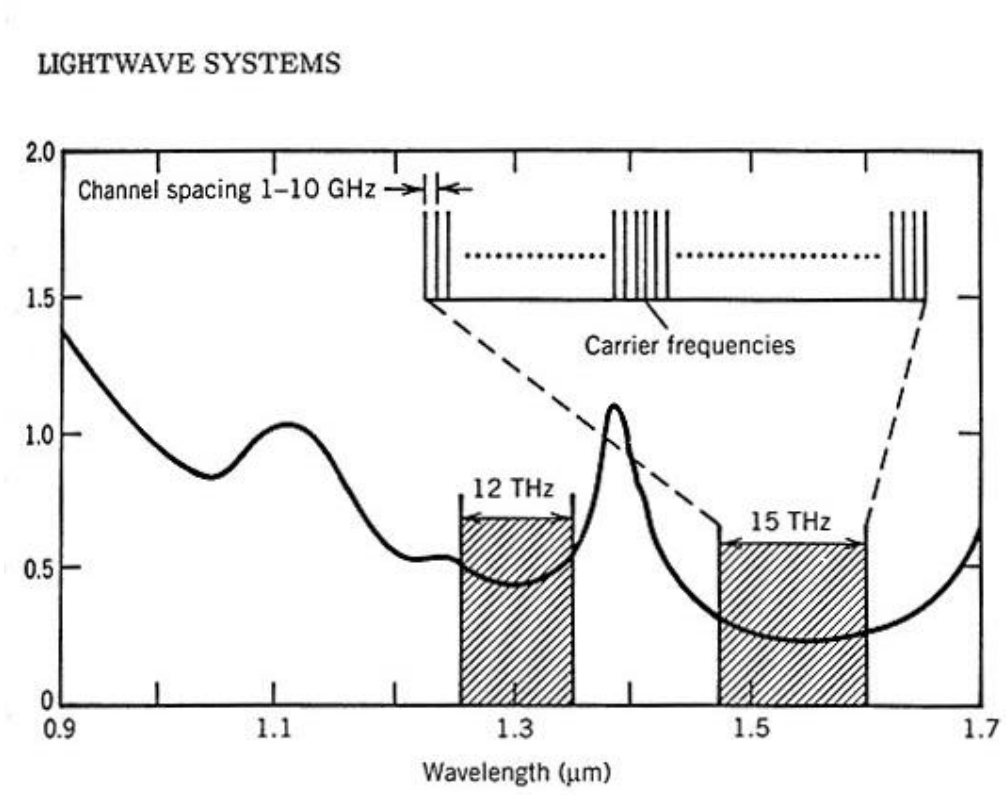

Figure 1.4 Low-loss transmission windows of silica fibers in the wavelength regions near 1.3 and 1.55ìm

The ultimate capacity of WDM fiber links depends on how closely channels can be packed in the wavelength domain. The minimum channel spacing is limited by the extent of interchannel crosstalk. Typically, channel spacing should exceed four times the bit rate. The low loss region of the state-of-the-art optical fibers extends over 120 nm in the wavelength region near 1.55ì m. The minimum channel spacing can be as small as 80 GHz or 0.6 nm for 20-Gb/s channels. Since 200 channels can be accommodated over the 120-nm bandwidth, the resulting effective bit rate can be as large as 4 Tb/s. if we assume that the WDM signal can be transmitted over 150 km without the need for electronic regeneration or optical amplification, the effective BL product exceeds 600 (Tb/s)-km with the use of WDM technology. This should be contrasted with third-generation commercial lightwave systems, which transmit a single channel over 80 km or so at a bit rate of up to 2.5 Gb/s, resulting in BL values of at most 0.2 (Tb/s)-km. Clearly, the use of WDM has the potential of improving the performance of fourth-generation lightwave systems by a factor of more than 1000.

In practice, many factors limit the use of the entire low-loss window extending over 120 nm. For example, optical amplifiers are often used to avoid electronic regeneration of the WDM signal. The number of channels is then limited by the bandwidth over which amplifiers can provide nearly uniform gain. The bandwidth of erbium-doped fiber amplifiers is limited to 30-35 nm even with the use of gain-flattening techniques. Among other factors that limit the number of channels are (1) stability and tenability of distributed feedback (DFB) semiconductor lasers, (2) signal degradation during transmission because of various nonlinear effects, and (3) interchannel crosstalk during demultiplexing. The commercialization of high-capacity WDM fiber links requires the development of many high-performance components, such as transmitters integrating multiple DFB lasers, channel multiplexers and demultiplexers with add-drop capability,

and large-bandwidth constant-gain amplifiers. Figure 1.5 shows schematically a WDM fiber link.

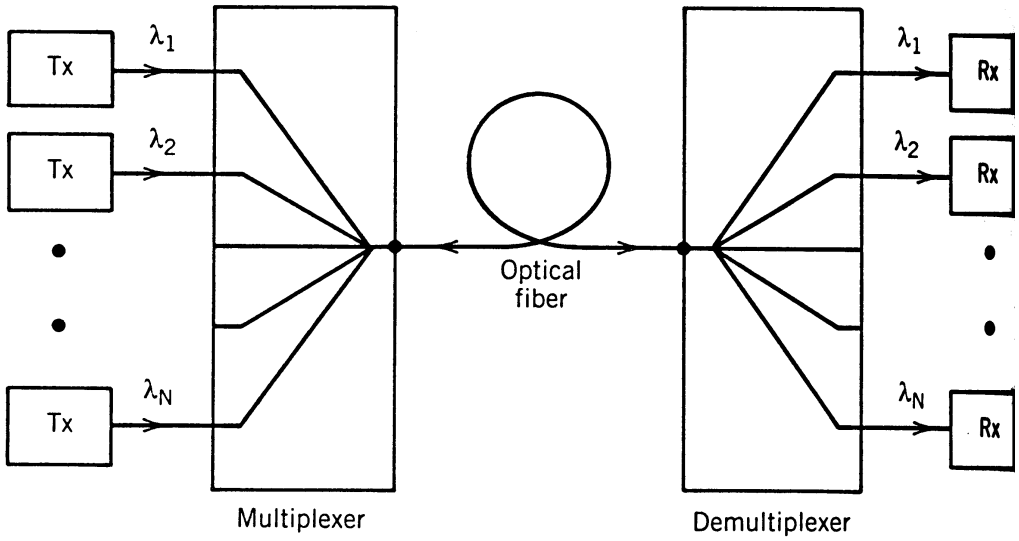

Figure 1.5 Multichannel point-to-point fiber link

1.3 Optical Amplifiers

For long-haul lightwave systems, the loss limitation has traditionally been overcome using optoelectronic repeaters in which the optical signal is first converted into an electric current and then regenerated using a transmitter. Such regenerators become quite complex and expensive for multichannel lightwve syhstems. An alternative approach makes use of optical amplifiers, which amplify the optical signal directly without requiring its conversion to electric domain. The use of optical amplifiers for long-haul lightwave systems became widespread during the 1990s. By 1996, optical amplifiers were a part of the fiber-optic cables laid across the Atlantic and Pacific oceans.

Optical amplifiers can serve several purposes in the design of fiber-optic communication systems as illustrated in Figure 1.6. The use of optical amplifiers is

particularly attractive for multichannel lightwave systems since they can amplify all channels simultaneously.

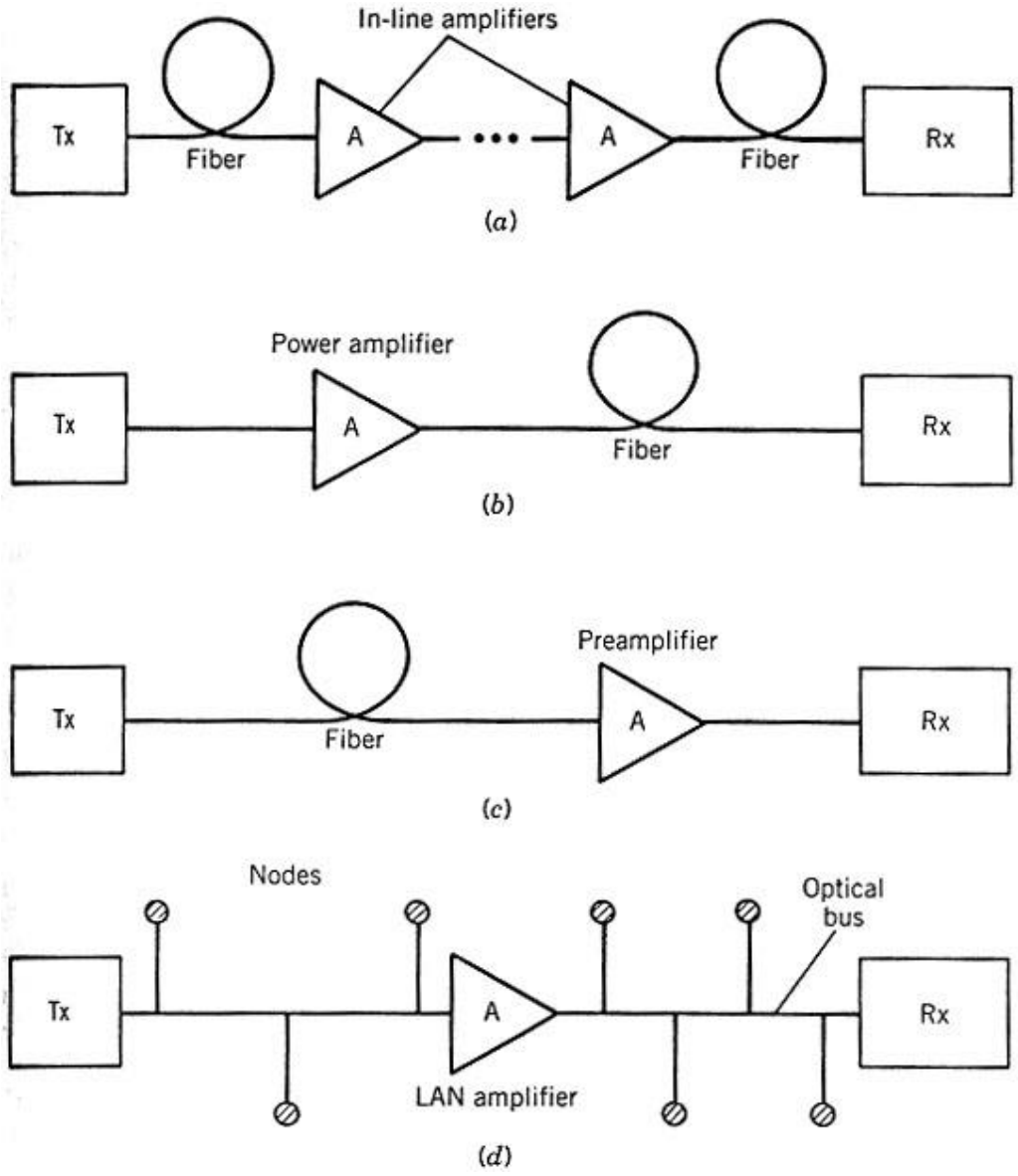

Figure 1.6 Four possible applications of optical amplifiers in lightwave systems: (a) as in-line amplifiers; (b) as a booster of transmitter power; (c) as a preamplifier to the receiver; (d) for compensation of distribution losses in local-area networks

Optical amplifiers amplify incident light through stimulated emission, the same mechanism as that used by lasers. Its main ingredient is the optical gain realized when the amplifier is pumped to achieve population inversion.

There are 4 kinds of different principle optical amplifiers: semiconductor laser amplifiers, fiber Raman amplifiers, fiber Brillouin amplifiers and doped-fiber amplifiers.

The optical gain, in general, depends not only on the wavelength of the incident signal, but also on the local beam intensity at any point inside the amplifier. Details of the frequency and intensity dependence of the optical gain depend on the amplifier medium. But usually, the gain curve is not flat with different wavelength. Figure 1.7 illustrates the gain spectrum of SLA and EDFA [1].

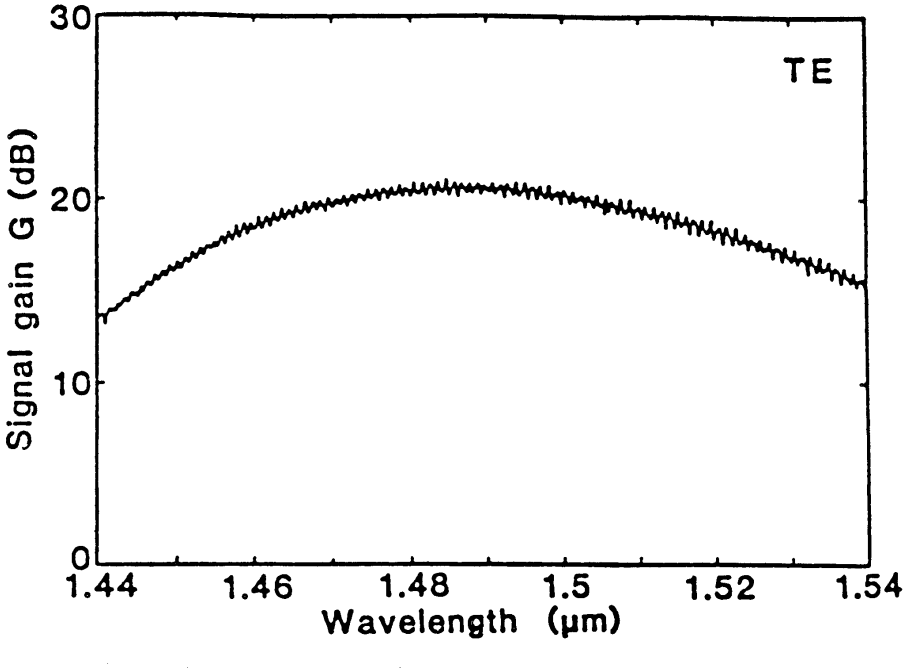

Figure 1.7(a) Amplifier gain versus signal wavelength for a semiconductor laser amplifier whose facets are coated to reduce reflectivity to about 0.04%

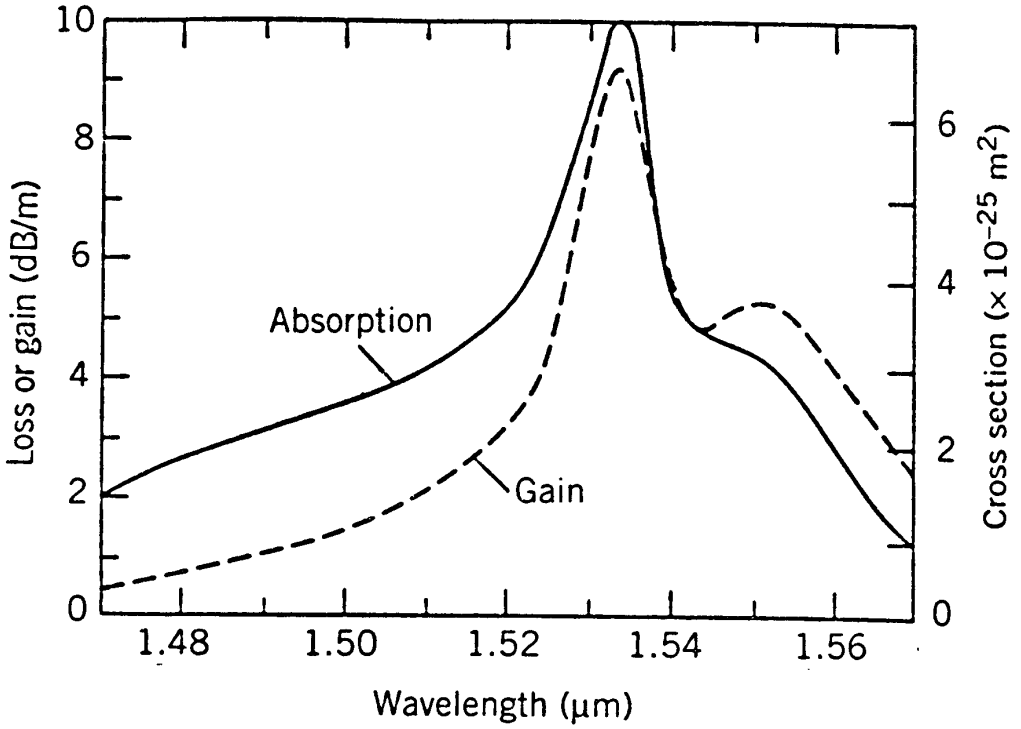

Figure 1.7(b) Absorption and gain spectra of an EDFA whose core was codoped with germania to increase the refractive index

1.4 Adaptive Equalizer/Attenuator

As fiber systems evolve to more channels, higher bit rates, and longer transparent spans, optical amplifiers are required to provide wider bandwidths, improved noise figures, and more precise control of the spectral gain characteristics. In the past, amplifiers for DWDM systems were typically designed to have a flat spectral gain over the bandwidth of interest, but some systems under development require an adjustable gain tilt to optimize system performance. The amplifier gain characteristics must also be stabilized against variations in operating parameters such as input power level and changes in the number of channels present. In active network, input power and amplifier gain change with time. Active level compensation at each wavelength is needed. An adaptive equalizer is a device with a chromatically variable transmissivity used to equalize channel powers in wavelength-division multiplexing (WDM) fiber-

optic communication lines [2]. Such a device has been realized by various technologies, such as MEMS [3, 4, 5], magneto-optic [6] and acousto-optic [7, 8] methods, planar lightwave circuits [9, 10, 11], holograms [12], etc. In the following section, several adaptive equalizer principles are presented.

1.4.1 MEMS based Adaptive Equalizer

J. E. Ford and J. A. Walker of Bell Labs demonstrated a dynamic WDM equalizer using a voltage-controlled variable reflectivity strip mirror and free-space wavelength mux to provide dynamic control over wavelength power levels across a continuous transmission spectrum [13]. The MARS (for mechanical anti-reflection switch) modulator shown in Figure 1.8 is basically a dielectric coating on a silicon substrate.

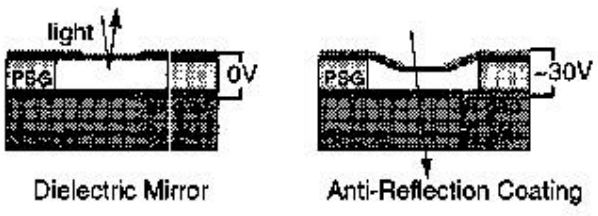

Figure 1.8 MARS micromechanical modulator

A silicon nitride $\frac{1}{4}l$ layer separated from the silicon substrate by a fixed $\frac{3}{4}l$ spacer acts as a dielectric mirror with about 72% reflectivity. Voltage applied to electrodes on top of the membrane creates an electrostatic force and pulls the membrane closer to the substrate. When the membrane gap is reduced to $\frac{1}{2}l$, the layer becomes an anti-reflection coating with close to zero reflectivity. This 0.4 micron vertical deflection is small compared to the 200 to 500 micron wide membrane. Electrically the device behaves as a tiny capacitor, with zero static power dissipation.

MARS modulators are used in a WDM equalizer by placing a row of modulators at the focal plane of a fiber-optic spectrometer and collecting the reflected light into an

output fiber. Figure 1.9 shows the picture of MARS variable reflectivity strip mirror, and Figure 1.10 shows the picture of such device. Figure 1.11 is its performance.

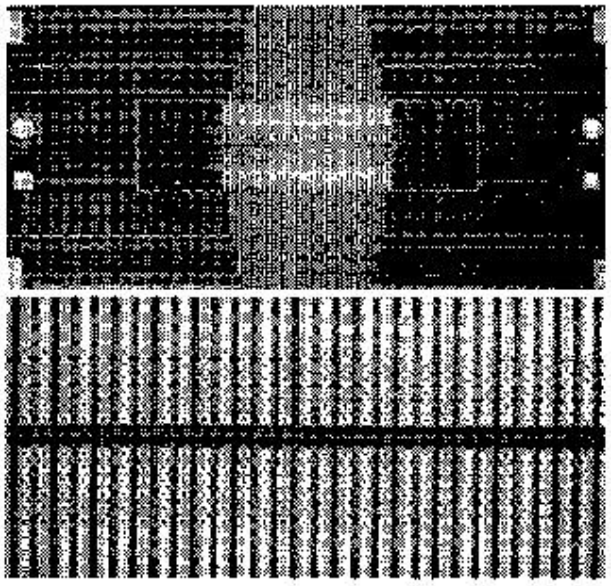

Figure 1.9 MARS variable reflectivity strip mirror

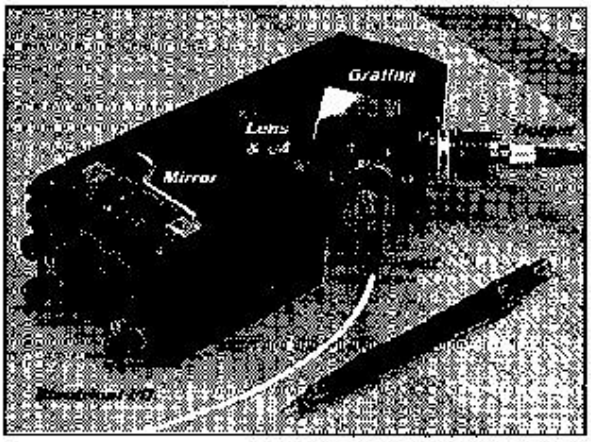

Figure 1.10 Picture of MARS system

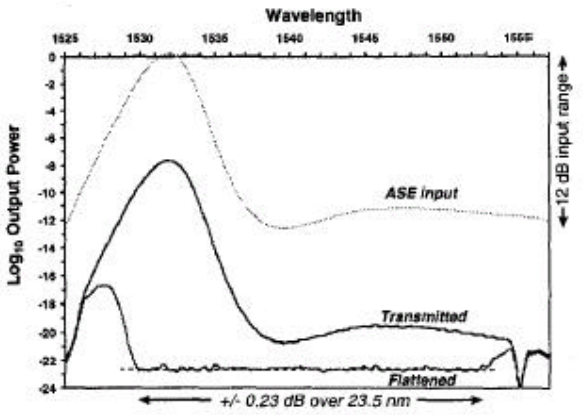

Figure 1.11 Equalized erbium fiber amplifier ASE

1.4.2 Optical Delay Line based Adaptive Equalizer

B. J. Offrein et al of IBM Research Division, Zurich Research Laboratory reported a device that are of the resonant coupler (RC) type, a cascade of power couplers and optical delay lines as shown in Figure 1.12 [14].

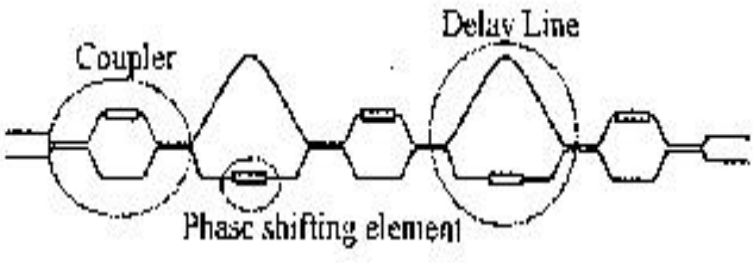

Figure 1.12 RC layout of 2 stages

Full controllability of the spectral response is obtained by making all cascaded elements adjustable. The phase change in the delay lines can be adjusted using the thermo-optic effect. The couplers are implemented as Mach-Zehnder interferometers with equal arm lengths, in which the power splitting ratio is set by tuning the phase in one arm. RC based components show a periodic response with a free spectral range set by the delay-line arm-length difference. The spectral details that can be flattened within one FSR depend on the number of delay line stages of the device. The channel

equalizer response and gain flattened filter response is shown in Figure 1.13 and Figure 1.14.

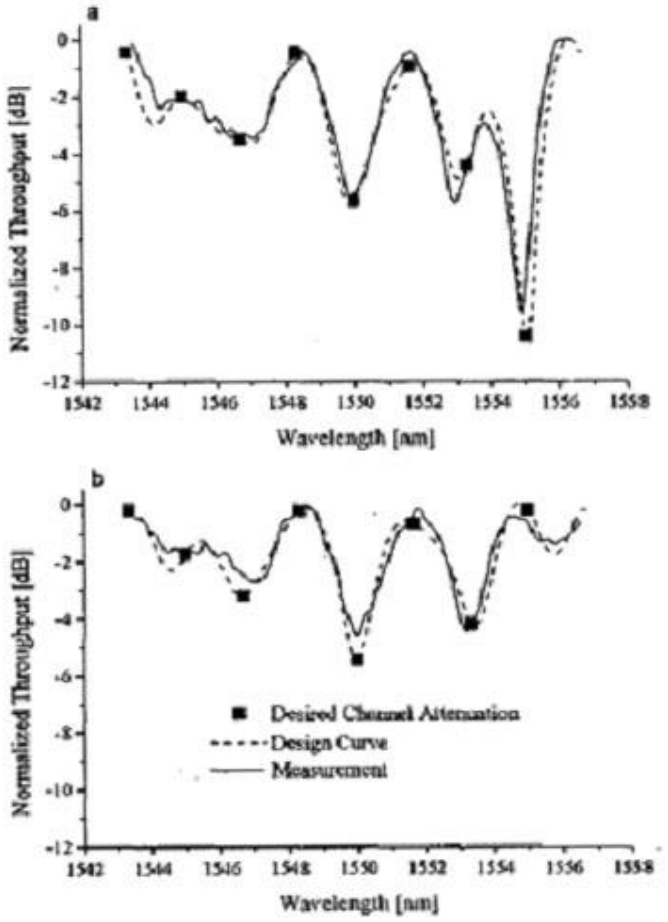

Figure 1.13 Channel equalizer response showing the individual attenuation of 8 channels

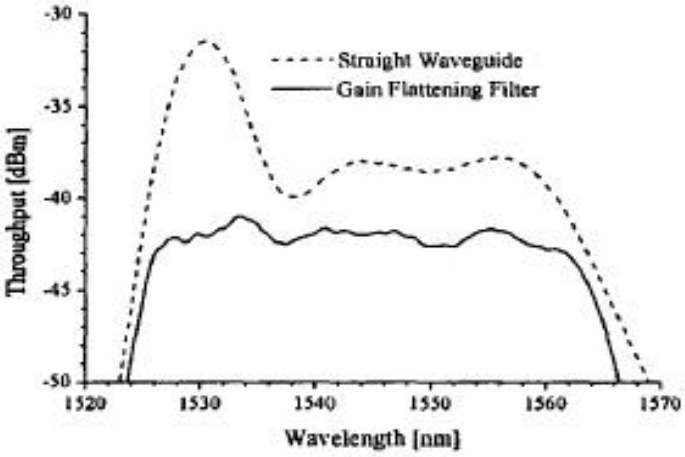

Figure 1.14 Gain flattened filter response

1.4.3 Phase-Shifter based Adaptive Equalizer

C. R. Doerr et al reported an adaptive equalizer, which is shown in Figure 1.15 [15].

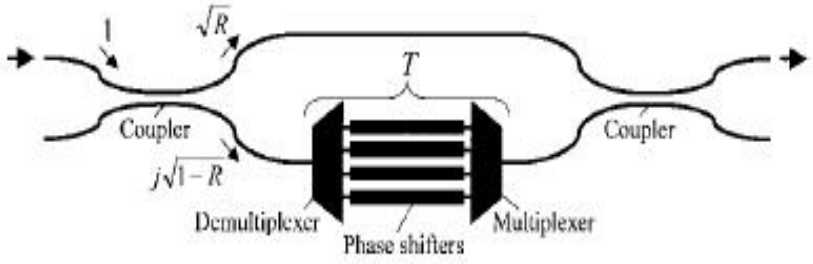

Figure 1.15 Diagram of the equalizer

The WDM channels enter from the left. Portions R and 1-R are sent to the upper and lower arms, respectively, and then recombine in the second coupler with the same splitting ratio. The upper arm is a simple waveguide, while the lower arm contains a demultiplexer and multiplexer connected by an array of programmable phase shifters. A programmable phase shifter is a device whose effective path length can be controlled externally. Assuming the couplers and waveguides have no excess loss, the transmissivity between the top left and right ports is $\{R+(1-R)\sqrt{T}\cos[f(p)]\}$, where $f(p)$ is the phase of the pth phase shifter. Thus the attenuation range (ratio of maximum to minimum attenuation) is $[\frac{R+(1-R)\sqrt{T}}{R-(1-R)\sqrt{T}}]^2$

The reflective design was made in InP, as shown in Figure 1.16.

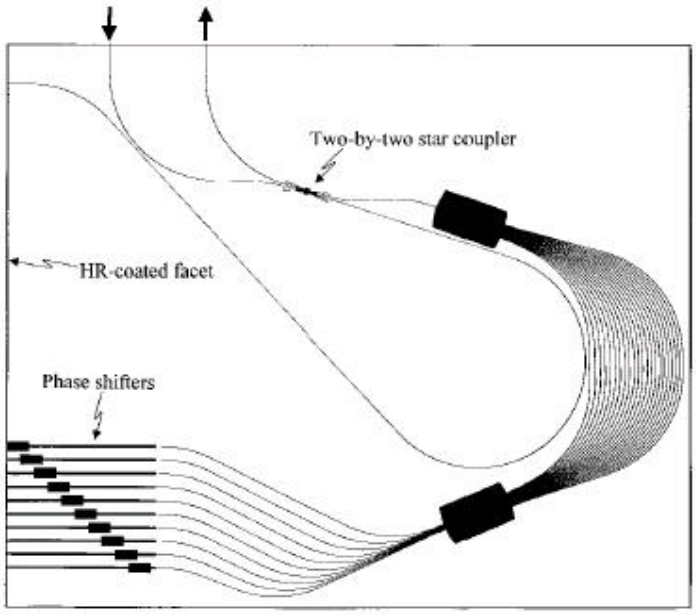

Figure 1.16 Layout of the equalizer

The demultiplexer/multiplexer is a conventional waveguide grating router (WGR) with ten channels spaced by 100 GHz, 22 grating arms, and a free-spectral range of 1600 GHz; the phase shifters are p-i-n junctions; and the coupler is a two-by-two star coupler. The optical signals enter the top left port. Half the power proceeds down the long curving waveguide (the "nonfiltered arm") reflects off the left-hand facet, and returns. The other half is demultiplexed by the WGR, proceeds through the phase shifters, reflects off the left-hand facet, and is remultiplexed by the WGR. The effective path lengths of the nonfiltered and filtered arms are equal to within a few micrometers. The returning powers interfere, and the amplitude of each passband that is sent to the top right port is controlled by the phase shifters. Results are shown in Figure 1.17.

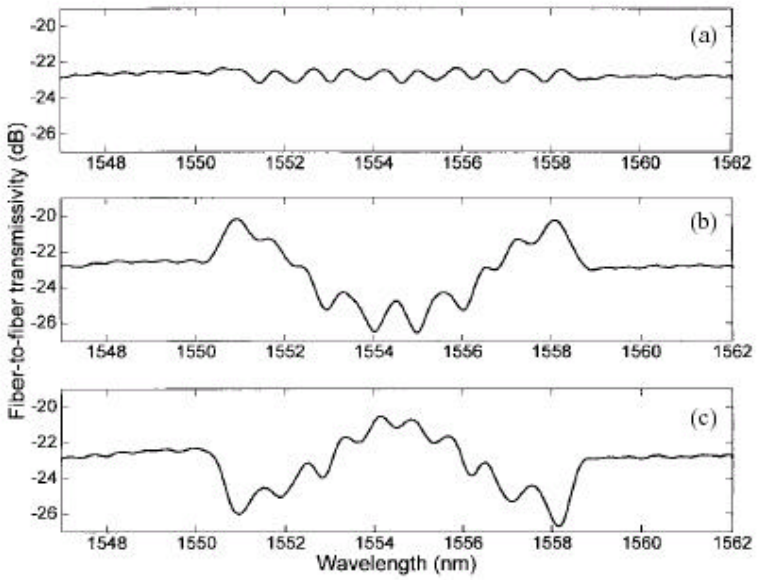

Figure 1.17 Measured fiber-to-fiber transmissivity of the equalizer versus wavelength of TE-polarized light for various phase-shifter settings. (a) All channels equal transmissivity. (b) Outer channels increased transmissivity. (c) Outer channels decreased transmissivity. The ten phase-shifter currents ranged from 0 to _16 mA. The plots were obtained by sending the spontaneous emission from an erbium-doped fiber amplifier in one port of the equalizer and measuring the exiting radiation from the other port with an optical spectrum analyzer, normalizing the measurement to the direct spontaneous emission spectrum. Resolution bandwidth= 0.1 nm.

1.5 Existing Deformable Mirror Technologies [16]

Figure 1.18 summarizes a comparison of the known deformable mirror technologies with the ideal specifications of a deformable mirror. Liquid crystal modulators are strictly not deformable mirrors, but they are reviewed for completeness. A discussion of the drawbacks of each technology, italicized in Figure 1.18, is presented in the following paragraphs.

1.5.1 Conventional Deformable Mirrors

Piezoelectric and electrostrictive actuators on deformable mirrors are the earliest and the most commonly used in adaptive optics systems today. The major disadvantage

is the lack of scalablity. These devices are fabricated by attaching an array of actuators to the back of a thin mirror by hand. This fabrication technique leads to large variability in device performance and difficulty achieving very large numbers of actuators at any reasonable cost. Furthermore, the actuator response is very temperature sensitive.

Characteristic	Ideal DM	PZT or PMN	Surface MEMS	Membrane DMs	Liquid Crystal
Throw (μm)	Large	4	~1	~10	~1
Spacing(mm)	Small	*7*	0.3	2	~0.1
Inter-actuator coupling	Low	Low	Low	*High*	Low
Influence Function	Smooth	Smooth	Smooth	Smooth	*Piston*
Cost	Low	*$1000 / actuator*	Low	Low	Low
Pixel Flatness	λ/50	Good	*Poor*	Good	Good
Roughness	Low	Low	*High*	Low	Low
Scalable to 1M Actuators	Yes	*No*	Yes	*No*	*No*
Circuitry Integration	Yes	*No*	*Maybe*	Yes	*Maybe*
Laser Power Handling	High	Good	*Poor*	Medium	*Poor*
Response Time (μs)	10	1000	15	1000	*10,000*
Fabrication Complexity	Low	*High*	Low	Low	Low
Thermal Sensitivity	Zero	*High*	Low	Low	*Medium*
Response to Voltage	Linear	Linear	Parabolic	Parabolic	*Nonlinear*

Figure 1.18 Summary of Existing Deformable Mirror Technology

1.5.2 Liquid Crystals

Liquid crystals offer a great deal of advantages to adaptive optics, but they offer no obvious way to address high bandwidth applications and offer very limited throw. Furthermore, the liquid crystal spatial phase modulators have difficulty handling laser power due to their absorbing indium tin oxide (ITO) transparent electrode. For example, data from Livermore National Laboratories shows that the damage threshold

of their liquid crystal spatial phase modulators is about 16W/cm2 for 1064nm light. 68 Temperature dependence of the liquid crystal material makes it necessary to operate in a limited temperature range. Finally, the performance of liquid crystal modulators is limited by chromatic and polarization effects for some applications.

1.5.3 Micromachined Deformable Mirrors

Silicon micromachining can be divided into surface micromachining techniques and bulk micromachining techniques. Surface micromachining involves adding layers of different materials to a wafer surface and then using a wet etchant to remove one type of layer and release the structure. In the typical case where these layers are polysilicon and silicon dioxide, the wetS etchant is hydrofluoric acid.

1.5.3.1 Surface Micromachining

Many researchers have developed surface micromachined deformable mirrors because they can be fabricated at foundries that do the processing of many different researchers in parallel instead of requiring each researcher to setup an expensive clean room to fabricate devices [17, 18]. Although surface micromachining offers a quick way to test architectures, the limitations of the process inhibit device performance. The surface quality of these devices has been poor due to the segmentation and perforation of the mirror surface. This perforation cannot be circumvented in the conventional surface micromachined process because a wet release must be able to enter the structure through the mirror surface. These perforations create high absorption points in the mirror and seed laser-induced damage.

Another limitation of surface micromachining is the inability to easily integrate complex silicon circuitry with surface micromachined devices. This leads to large numbers of densely packed wires on a wafer. This, in turn, could provide a fundamental limit to the scaling of these mirrors to large sizes. In addition to the large numbers of

wires on a surface micromachined wafer without any circuitry, there is the further problem of getting connections to these wires off the chip. Finally, accumulated roughness and stresses induced during deposition of the layers make it difficult to achieve high quality mirror surfaces, even if the wafer is polished before the wet etch release step [18].

Typical foundry surface micromachining, like that used by Boston University and Boston Micromachines, has a limited thickness and therefore a limited throw. A recent advance in surface micromachining from Lucent has demonstrated the ability to achieve longer throw surface micromachined devices by exploiting the difference in stresses of two coatings. Upon release, the Lucent mirrors lift above the surface allowing for a wider range of tilt. The disadvantage of this technology is that the differential stress elements used for lifting the mirror are temperature sensitive.

1.5.3.2 Bulk Micromachining

Bulk micromachining always involves deep etches into the wafer, often completely through the wafer. When done properly, the deep etch enters the back of the mirror and leaves the front reflective surface untouched during processing. Typically long etches in tetra-methyl ammonium hydroxide (TMAH) or potassium hydroxide (KOH) are used for removing large amounts of silicon with silicon nitride or silicon dioxide as an etch mask. Recently, many researchers have adopted deep reactive ion etching (DRIE) to do bulk micromachining instead of the wet etching because it offers more control of the shape of the etching. Bulk micromachining offers the ability to achieve a continuous membrane surface, which would alleviate scattering problems with surface micromachining. Unfortunately the majority of the mirrors to date made using this technology do not scale to large apertures because the mirror resonance frequency scales inversely with the mirror radius. Furthermore, the cross talk between actuators is

high, thus preventing high-order wavefront correction. Finally, current bulk micromachined deformable mirrors are typically destroyed during electrostatic snap-down, which occurs when the electrostatic force exceeds the mechanical restoring force and the mirror collapses into the underlying pad arrays. Integration of addressing circuitry is typically easier with bulk micromachined devices since the circuitry can be made in a separate run and bonded to the micromachined structure using a low-temperature bond that does not damage the circuitry.

Many complex structures can be made in even a simple clean room with 1970's class equipment. Complex steps like epitaxial silicon growth or silicon nitride deposition can be sent out to a number of different foundries for minimal cost. Simple steps like lithography can be performed in a number of small clean rooms nationwide. Finally, the cost of setting up a small clean room for bulk micromachining is typically small and several of these clean rooms allow users to lease space for very reasonable rates.

Chapter 2 Fourier Analysis of Multi-Beam Interference

2.1 Introduction to Multi-Beam Interference

A basic understanding of a signal waveform is that it can be decomposed onto and reconstructed by a set of orthogonal basis vectors in the vector space. *Fourier transform* is a specification of the above idea. It decomposes a waveform into sinusoids of different frequencies with different amplitudes. And we can use the spectrum to reconstruct the waveform.

The orthogonal basis can be written as:

$\{1,\exp(\pm jw_1 t),\exp(\pm jw_2 t),...,\exp(\pm jw_3 t),...\}$. Given a time domain signal $f(t)$, its *Fourier transform pair* is:

$$\begin{cases} F(w) = FT\{f(t)\} = \int_{-\infty}^{+\infty} f(t)\exp(-jwt)dt \\ f(t) = IFT\{F(w)\} = \frac{1}{2p}\int_{-\infty}^{+\infty} F(w)\exp(jwt)dw \end{cases} \quad (2.1)$$

Similarly, a multi-beam interference spectrum can be analyzed in a vector space by *Fourier transform*. Suppose a plane wave of monochromatic light is incident upon a plane-parallel transparent plate of refractive index n' surrounded by a medium of refractive index n at angle q as shown in Figure 2.1. Let *r* be the reflection coefficient, and *t* the transmission coefficient for wave traveling from the surrounding medium into the plate; and let *r', t'* be the reflection and transmission coefficients for wave traveling from the plate to the surrounding medium.

$$E_0 = tt'E^{(i)},\ E_1 = tt'r'^2E^{(i)}e^{-jd},\ E_2 = tt'r'^4E^{(i)}e^{-j2d},\ldots,\ E_p = tt'r'^{2p}E^{(i)}e^{-jpd},\ldots (2.2)$$

$$E^{(t)} = \sum_{p=0}^{\infty} E_i \quad (2.3)$$

$E^{(i)}$ is the complex amplitude of the incident light, and $E^{(t)}$ is the complex amplitude of the transmitted light. *r, r', t, t'* are given in terms of *n, n', q* and q' by the Fresnel formulae. $d = \frac{4p}{l} n'h\cos q' = wL'$.

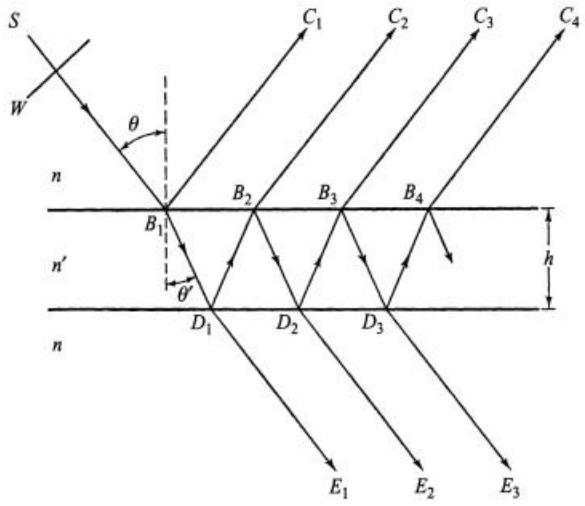

Figure 2.1 Reflection and transition of a plane wave in a plane-parallel plate

The complex amplitude of the transmitted light $E^{(t)}$ can be written as:

$$E^{(t)}(w) = \sum_{p=0}^{\infty} a_p \exp(-jT_p w) \quad (2.4)$$

where $a_p = tt'r'^{2p}E^{(i)}$ is the complex magnitude of pth beam, $T_p = 2pn'h\cos q'/c$ is the relative time delay of pth beam to the assumed zero time delay beam, and wT_p gives the relative phase difference of the pth beam and the zero time delay beam.

Equation (2.4) is very similar to *Discrete Time Fourier Series*. As we will see, *Fourier transform* is a very powerful tool in the analysis of multi-beam interference, and also in the design of multi-beam interference devices to obtain a target spectrum. In this chapter, time domain signal *Fourier transform* is first presented, and how to map the concept of *Fourier transform* to multi-beam interference is discussed.

2.2 Fourier Transform Analysis of Multi-Beam Interference

A general understanding of a signal waveform is that it can be decomposed onto and reconstructed by a set of orthogonal basis vectors in the vector space. The number *n* of the dimensions of the vector space can be finite or infinite.

Assume we have a set of orthogonal basis: $\{s_1(t), s_2(t), s_3(t), ..., s_i(t), ...\}$.

$$< s_i(t), s_j(t) >= \int_{-\infty}^{+\infty} s_i(t) s_j^*(t)\, dt = d(i-j) \quad (2.5)$$

$$\left\| s_i(t) \right\| = \int_{-\infty}^{+\infty} s_i(t)\, s_i^*(t)\, dt = 1, i = 1,2,..., k, ... \quad (2.6)$$

Thus signal $f(t)$ can be expressed as:

$$f(t) = \sum_{i=1}^{+\infty} s_i s_i(t) \quad (2.7)$$

where

$$s_i =< f(t), s_i(t) >= \int_{-\infty}^{+\infty} f(t) s_i^*(t) dt \quad (2.8)$$

Fourier transform is a specification of the above idea. *Fourier transform* decomposes a waveform into sinusoids of different frequencies with different amplitudes. And we can use the spectrum to reconstruct the waveform.

The orthogonal basis can be written as: $\{1, e^{\pm jw_1 t}, e^{\pm jw_2 t}, ..., e^{\pm jw_i t}, ...\}$. Given a time domain signal $f(t)$, its *Fourier transform* is:

$$F(w) = FT\{f(t)\} = \int_{-\infty}^{+\infty} f(t) e^{-jwt} dt \quad (2.9)$$

$$f(t) = IFT\{F(w)\} = \frac{1}{2p} \int_{-\infty}^{+\infty} F(w) e^{jwt} dw \quad (2.10)$$

Figure 2.2 shows the *Fourier transform* of the window function.

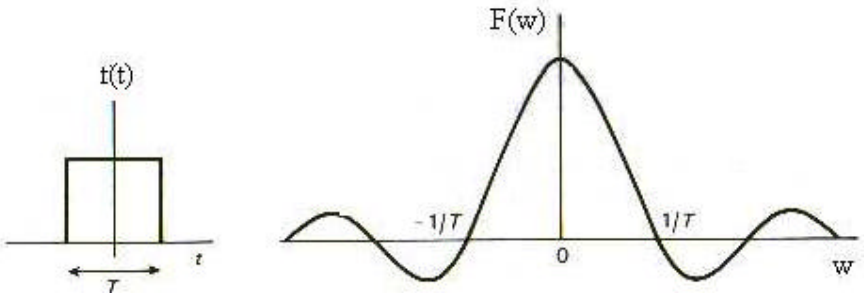

Figure 2.2 Fourier transform of a time domain signal f(t)

Similarly, a multi-beam interference spectrum can be analyzed in a vector space by *Fourier transform*. Let's begin with a Fabry-Perot cavity as shown in Figure 2.1.

The math picture of Equation (2.4) is that an electric field spectrum $E(w)$ can be decomposed to a set of orthogonal basis $\{1, e^{-jT_1w}, e^{-jT_2w}, e^{-jT_3w}, ...\}$

$$< e^{-jT_iw}, e^{-jT_jw} >= \int_{-\infty}^{+\infty} e^{-jT_iw} (e^{-jT_jw})^* dw = d(T_i - T_j) \quad (2.11)$$

The physics meaning of the basis vector is the relative delay of each beam to the assumed zero relative delay beam. Beams with the same relative delay are orthogonal and totally correlated.

The weight of each basis is given by:

$$a_p =< E(w), e^{-jT_pw} >= \int_{-\infty}^{+\infty} E(w)(e^{-jT_pw})^* dw \quad (2.12)$$

And the electric field spectrum $E(w)$ thus can be reconstructed:

$$E(w) = \sum_{p=0}^{\infty} a_p e^{-jT_pw} \quad (2.13)$$

The physics interpretation of this math picture is that: in multi-beam interference, we arbitrarily choose one beam and assume it has a delay of zero: $T = 0$. All other beams have different relative delay to this beam: $\{T_1, T_2, ...\}$. These different relative delay form a set of orthogonal basis (Equation 2.11). $E(w)$ can be decomposed in this vector space. Equation (2.12) gives the amplitude of each basis—electric field

amplitudes of respective beams with different relative light paths. Thus, $E(w)$ can be reconstructed by this orthogonal basis followed by Equation (2.13).

Equations (2.12) and (2.13) apply for discrete T values. If T takes the continuous form, then the above formulas take the form of:

$$A(T) = \int_{-\infty}^{+\infty} E(w) e^{-jTw} dw \quad (2.14)$$

$$E(w) = \frac{1}{2p} \int_{-\infty}^{+\infty} A(T) e^{jLw} dT \quad (2.15)$$

Equations (2.14) and (2.15) are the general form. It tells us the relationship between an electric field spectrum $E(w)$ and the relative delay of beams involved in multi-beam interference. It tells us that any electric field spectrum $E(w)$ can be seen and get as the result of multi-beam interference. The complex amplitude $A(T)$ of the beam with the relative delay T is given by Equation (2.14). Once we have $A(T)$, we can reconstruct $E(w)$.

$$\begin{cases} f(t) \xrightarrow[IFT]{FT} F(w) \\ E(w) \xrightarrow[IFT]{FT} A(T) \end{cases} \quad (2.16)$$

2.3 Properties of Multi-Beam Interference

In time domain signal processing, *Fourier transform* is the bridge between Time domain and Frequency domain. It provides us another prospective to understand the signal. Lots of signal properties that are hard to understand in time domain are apparent in frequency domain. Similarly, *Fourier transform* is the bridge between the multi-beam interference electric field amplitude spectrum domain and relative delay T domain. It gives us another angle to look at multi-beam interference. Some properties of interference spectrum are apparent in T domain.

Example 1.In multi-beam interference, if we want light of all frequencies suffer no loss, how do we design the relative delay T?

Normalized $E(w)$ has an amplitude of 1. $FT\{1\} = d(T)$. This means the beams should all have the same delay. This result matches our experience in ideal mirror reflection.

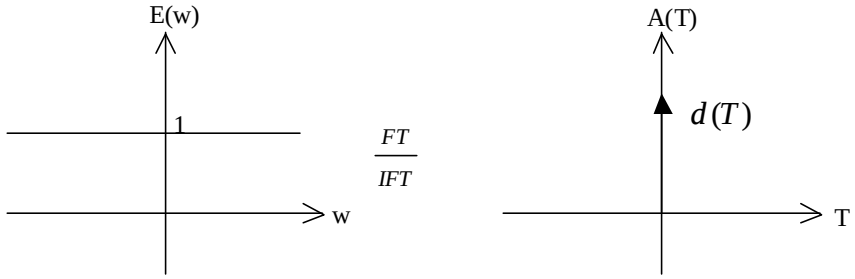

Figure 2.3 Example of ideal mirror reflection

Example 2.How do we understand Fabry-Perot cavity multi-beam interference in T domain?

The ideal transmitted intensity spectrum $I(w)$ is drawn in Figure 2.4(a). $I(w) = E(w)E^*(w)$, $E(w) = FT\{A(T)\}$. It has a spectrum line width $dw \to 0$. From the theory of *Fourier transform* of sampled time domain signal, we get $A(T)$ as shown in Figure 2.4(a). Note that every component of $A(T)$ has the same amplitude, and the number of the components is infinite. It means if we want a $I(w)$ to have $dw \to 0$, we have to make the energy reflection ratio *R* close to 100%, so that each beam has the same energy, and we have to take infinite number of beams into account. This result matches our experience.

In Figure 2.4(b), if we have *R* still large but not close to 100%, each component of $A(T)$ will be modulated by Equation (2.12). The envelope function is:

$$A_{envelope}(T) = tt' r'^{2T/T'} \quad (2.17)$$

where $T' = 2n'h\cos q' / c$

From the theory of *Fourier transform* of sampled time domain signal, we know the intensity of the *Inverse Fourier transform* of $A_{envelope}(T)$ is the basic unit of the periodic $I(w)$ of the Fabry-Perot cavity, as shown in Figure 2.4(c). This explains why $I(w)$ has a small but none-zero dw_1.

In Figure 2.4(d), we have *R* small. Again, $A_{envelope}(T)$ is given by Equation (2.17), but of different shape due to the difference of *R*. This results in a larger dw_2.

$A_{envelope}(T)$ and its intensity of *Inverse Fourier transform* is plotted in Figure 2.4(e).

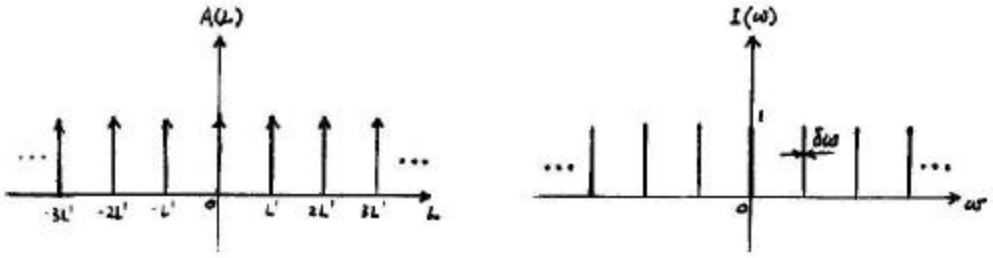

Figure 2.4(a) R=100%

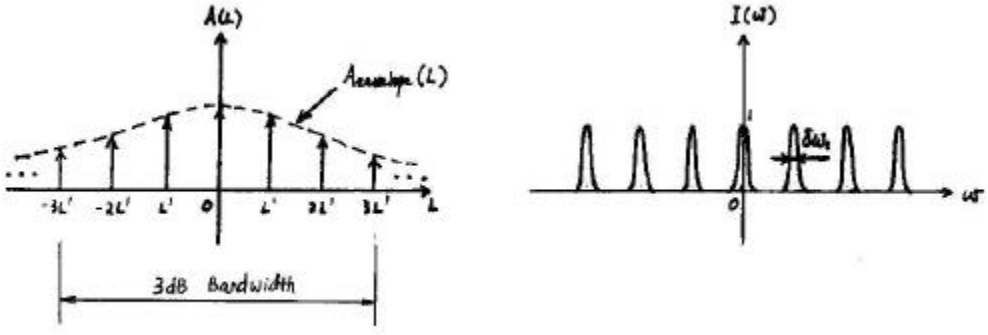

Figure 2.4(b) R is high

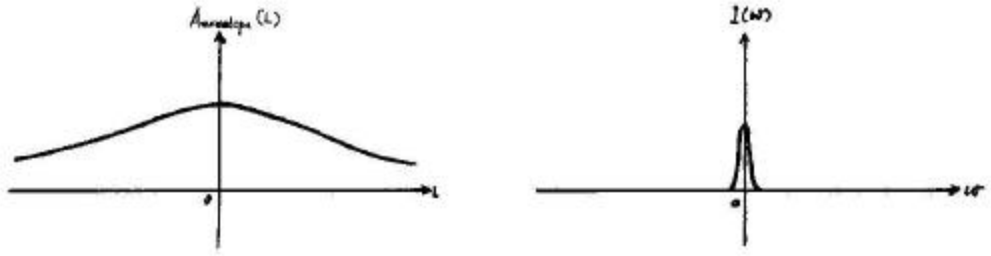

Figure 2.4(c) Relation of $A_{envelope}(T)$ and single unit of $I(w)$

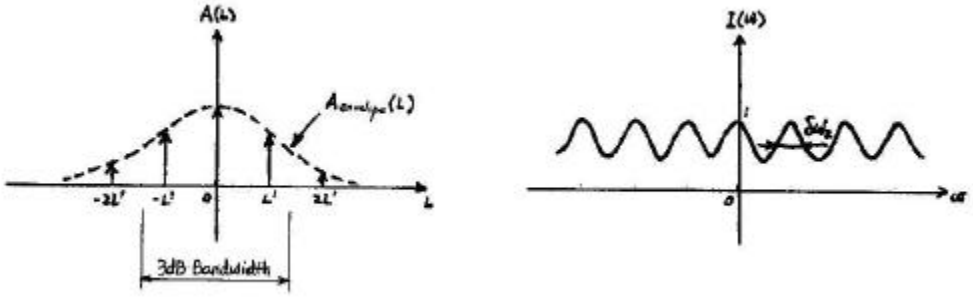

Figure 2.4(d) R is low

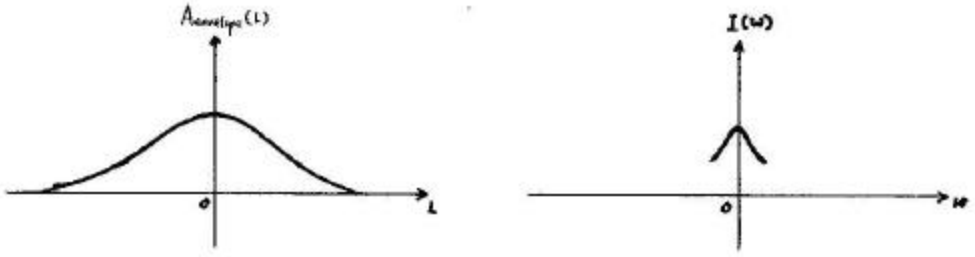

Figure 2.4(e) Relation of $A_{envelope}(T)$ and single unit of $I(w)$

The above theoretical analysis matches the well-known results given in many textbooks, such as “Principles of Optics”. Figure 2.5 shows the transmission spectrum of the Fabry-Perot cavity due to different R.

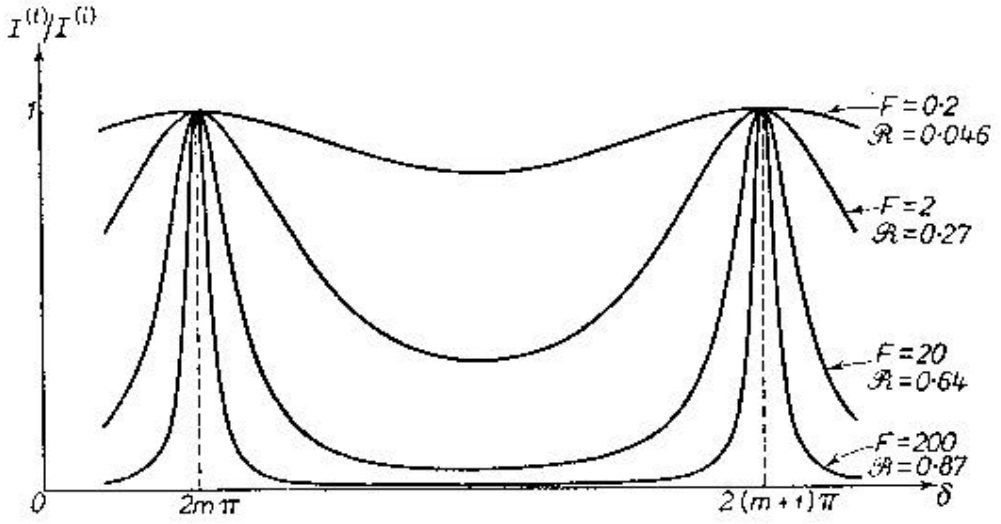

Figure 2.5 Transmission spectrum of the Fabry-Perot cavity due to different R

In time domain signal analysis, the concept of bandwidth is used. In time signal reconstruction, the more the bandwidth, the more the detail of reconstructed signal. Figure 2.6 shows the relation of bandwidth to signal detail.

Similarly, we introduce the concept of bandwidth in *Fourier analysis* of multi-beam interference. What we mean bandwidth now is how many different T's included. The more the bandwidth, the more the detail of the interference spectrum. The relation of bandwidth to spectrum detail is plotted in Figure 2.7.

Figure 2.6(a) small bandwidth and reconstructed signal

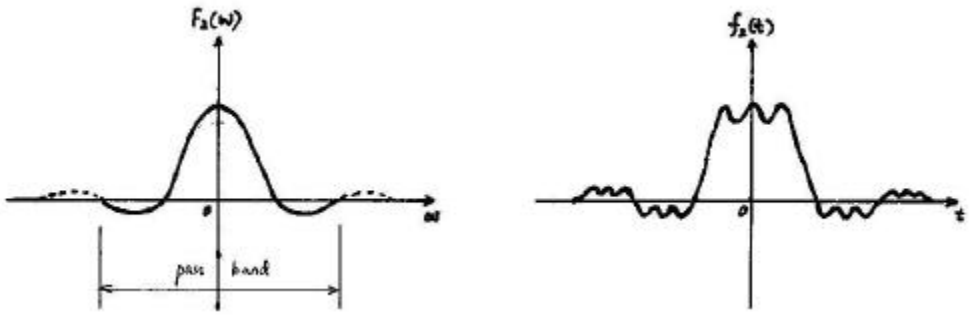

Figure 2.6(b) big bandwidth and reconstructed signal

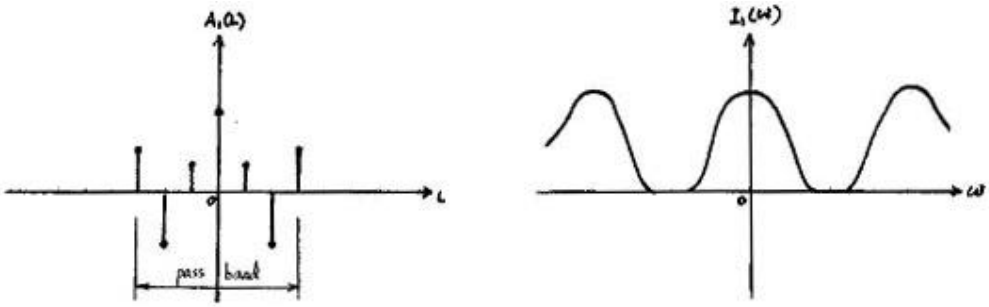

Figure 2.7(a) small bandwidth and reconstructed spectrum

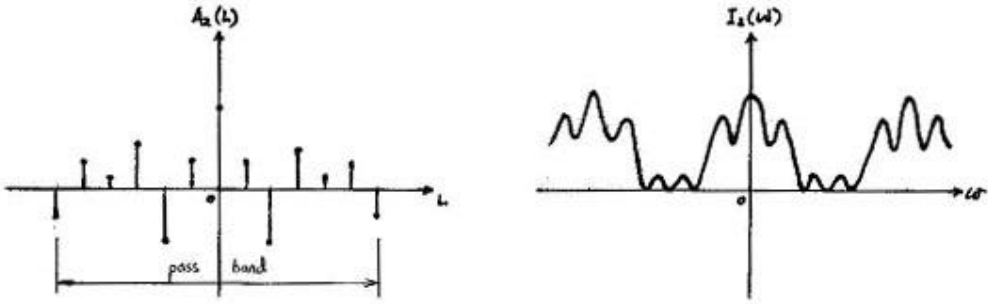

Figure 2.7(b) big bandwidth and reconstructed spectrum

We can use bandwidth to analyze Figure 2.4(a), (b) and (d). (a) has infinite bandwidth. This is why its spectrum reflects all the details. (b) has bandwidth smaller than (a) but larger than (c). So it can reflect medium details of spectrum. (c) has poor bandwidth. It can only reflect general changes of spectrum.

The concept of bandwidth is very important in *Fourier analysis* of multi-beam interference. It tells us what is the limit of a particular multi-beam interference device.

What kind of spectrum detail a multi-beam interference device can provide is largely related to how large the range of T the device can provide. This will provide us as a guide to choose and design the multi-beam interference device.

Chapter 3 Principles of Multi-Beam Interference Design

Fourier transform is a powerful tool in transverse problems. The principle of multi-beam interference design is presented below.

Multi-beam interference can be written as:

$$E(w) = \frac{1}{2p}\int_{-\infty}^{+\infty} A(T)e^{jTw}dT \quad (3.1)$$

$$I(w) = E(w)E^{*}(w) = |E(w)|e^{-jj(w)}|E(w)|e^{jj(w)} = |E(w)|^2 \quad (3.2)$$

In real application, we need to design the structure parameters $\{A(T)\}$ and $\{T\}$ to realize a given target intensity spectrum $I(w)$ on a particular frequency span $[w_1, w_2]$. $\{A(T)\}$ is a set of complex amplitudes—$\{|A(T)|e^{-jj_T}\}$. But in reality, it is hard to manage a constant phase shift j_T for all light frequencies w. What we can realize in physics is real amplitudes $\{|A(T)|\}$.

$E(w)$ is the bridge between target $I(w)$ and the implementable multi-beam interference. Equation (3.2) shows that $E(w)$ with different $j(w)$ but same modules $|E(w)|$ have the same $I(w)$. There is a possibility that we find one $E(w) = |E(w)|e^{-jj(w)}$ which has real *Fourier transform* $A(T)$ and target spectrum $I(w)$.

Fourier transform theory shows a real and even function has real and even *Fourier transform*. A real even and imaginary odd function has real *Fourier transform*.

Since phase information $j(w)$ of $E(w)$ is lost in $I(w)$ and hard to reconstruct, a better way to have real $A(T)$ is to have real and even $E(w)$. Such $E(w)$ forces the real $A(T)$ to be even, which means if a beam with relative delay T_i of electric field

amplitude $A(T_i)$ participated the interference, another beam with relative delay $-T_i$ of electric field amplitude $A(-T_i) = A(T_i)$ must also participate the interference.

$$\begin{aligned} E(-w) &= E(w) \\ A(-T) &= A(T) \\ E(w) &= \frac{1}{2p}\int_{-\infty}^{+\infty} A(T)e^{jTw}dT \end{aligned} \qquad (3.3)$$

The procedure of designing target spectrum $I(w)$ is:

1. In real application we are interested in intensity spectrum on a particular frequency span $[w_1, w_2]$, but not the whole spectrum $I_{whole}(w)$ [Figure 3.1(a)]. The rest of the spectrum could be arbitrary. Thus what we need is only to construct a multi-beam interference whose intensity spectrum matches the target spectrum on that particular frequency span. There are no restrictions on other part of the interference spectrum. This understanding would bring much convenience. For mathematical clearance, we define target $I(w)$:

$$\Pi(\frac{w}{\Delta w}) = \begin{cases} 1, |w| \le \dfrac{\Delta w}{2} \\ 0, |w| > \dfrac{\Delta w}{2} \end{cases} \qquad (3.4)$$

$$I(w) = I_{whole}(w)\Pi(\frac{w - w_c}{\Delta w}) \qquad (3.5)$$

where $w = 2pc/l, w_c = (w_1 + w_2)/2, \Delta w = w_2 - w_1$

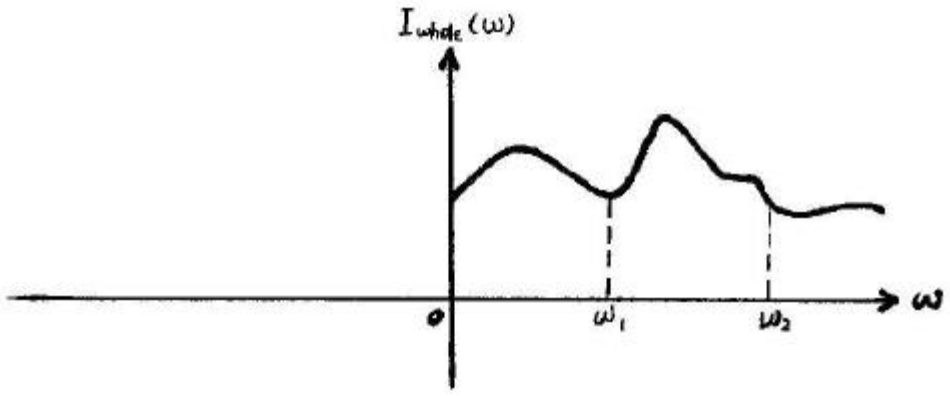

Figure 3.1(a) $I_{whole}(w)$

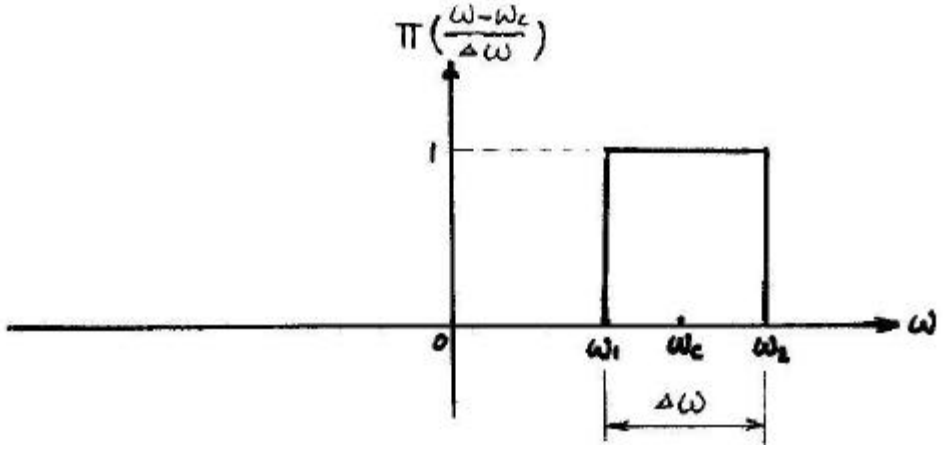

Figure 3.1(b) $\Pi(\frac{w-w_c}{\Delta w})$

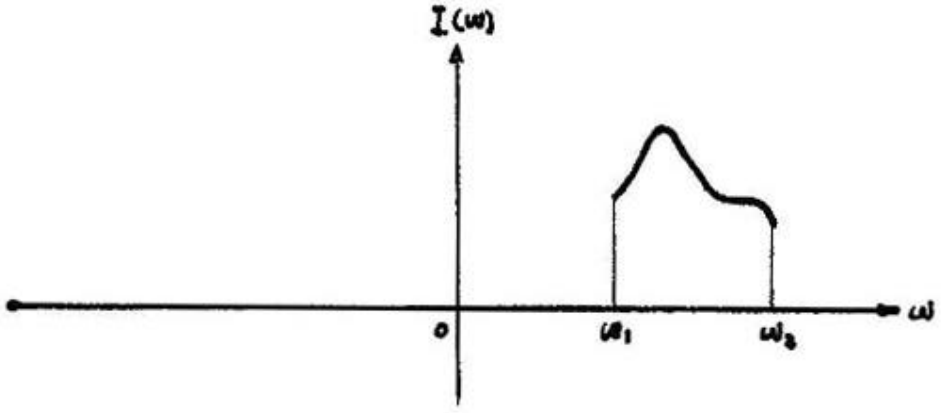

Figure 3.1(c) target spectrum $I(w)$

2. Use target $I(w)$ to construct real and even $I_{even}(w)$

$$I_{even}(-w) = I_{even}(w) \quad (3.6)$$

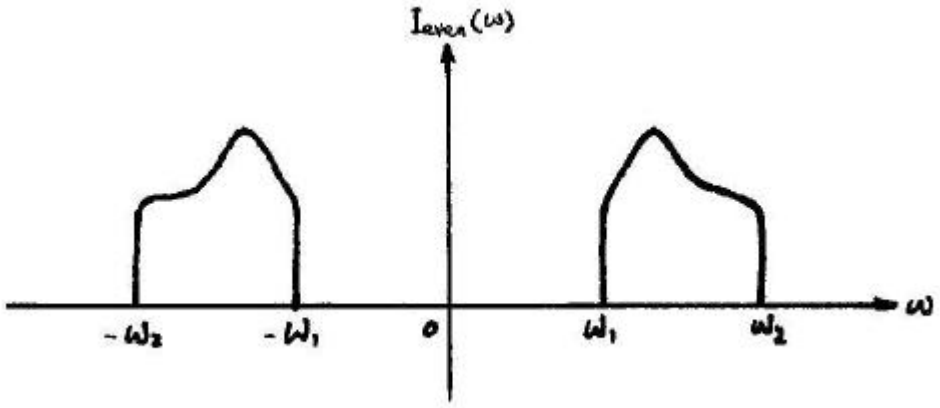

Figure 3.1(d) $I_{even}(w)$

3. Get $E_{even}(w)$ by

$$\begin{cases} E_{even}(w) = \sqrt{I_{even}(w)} \\ E_{even}(-w) = E_{even}(w) \end{cases} \quad (3.7)$$

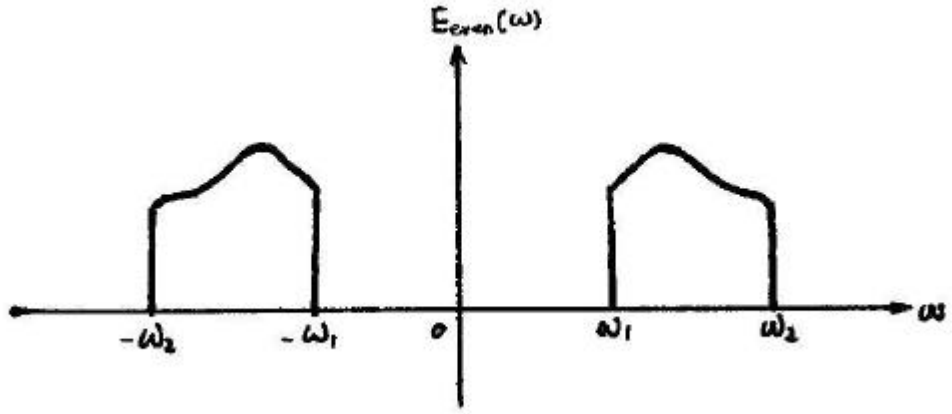

Figure 3.1(e) $E_{even}(w)$

4. Get real and even $A(T)$ by *Fourier transform*

$$A(T) = FT\{E_{even}(w)\} = \int_{-\infty}^{+\infty} E_{even}(w) e^{-jTw} dw \quad (3.8)$$

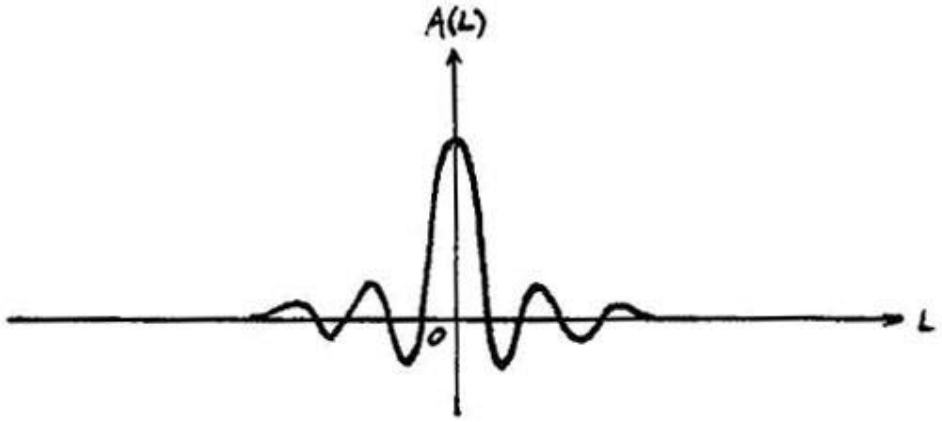

Figure 3.1(f) $A(T)$

Negative $A(T)$ can be realized by introducing an additional phase shift of p. In real application the bandwidth is very small compared to the center wavelength, that is:

$$\frac{\Delta w/2}{w_c} = e \prec\prec 1 \quad (3.9)$$

We can introduce an additional half-wave relative time delay:

$$T_p = p \Big/ w_c \quad (3.10)$$

to the beams with negative $A(T)$:

$$\begin{aligned} & A(T_i)\exp[-jw(T_i+T_p)] = -A(T_i)\exp(-jT_iw)\exp(-j\frac{w-w_c}{w_c}p) \\ & = -A(T_i)\exp(-jT_iw)[\cos(\frac{w-w_c}{w_c}p) + j\sin(\frac{w-w_c}{w_c}p)] \end{aligned} \quad (3.11)$$

The factor $\cos[p(w-w_c)/w_c] + j\sin[p(w-w_c)/w_c]$ introduces distortion. The maximum distortion occurs at $w = w_c \pm \Delta w/2$:

$$\begin{cases} \sin(\dfrac{w_c \pm \Delta w/2}{w_c}p) = \sin(p) + \dfrac{\sin'(p)}{1!}(\pm ep) + \dfrac{\sin''(p)}{2!}(\pm ep)^2 + \ldots \approx 0 \\ \cos(\dfrac{w_c \pm \Delta w/2}{w_c}p) = \cos(p) + \dfrac{\cos'(p)}{1!}(\pm ep) + \dfrac{\cos''(p)}{2!}(\pm ep)^2 + \ldots \approx 1 \end{cases} \quad (3.12)$$

Distortion can be omitted for very small e. For instance, in fiber communication, the Erbium-doped fiber amplifiers (EDFAs) usually has a central wavelength of $l_c = 1550nm$ and an amplify range of $\Delta l = 30nm$. The maximum distortion is:

$$-A(T_i)\exp(-jT_iw)[\cos(\frac{\Delta l/2}{l_c - \Delta l/2}p) + j\sin(\frac{\Delta l/2}{l_c - \Delta l/2}p)]$$
$$= -A(T_i)\exp(-jT_iw)(0.9995 + j0.0307) \approx -A(T_i)\exp(-jT_iw)$$

5. Use $\{A(T)\}$ and $\{T\}$ as the structure parameters of multi-beam interference to construct $E_{con}(w)$:

$$E_{con}(w) = IFT\{A(T)\} = \frac{1}{2p}\int_{-\infty}^{+\infty} A(T)e^{jTw}dT \quad (3.13)$$

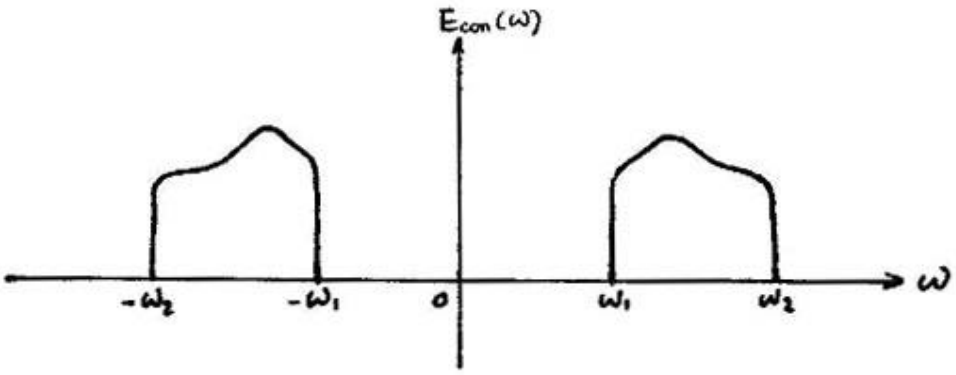

Figure 3.1(g) $E_{con}(w)$

6. $I_{con}(w) = E_{con}^2(w)$

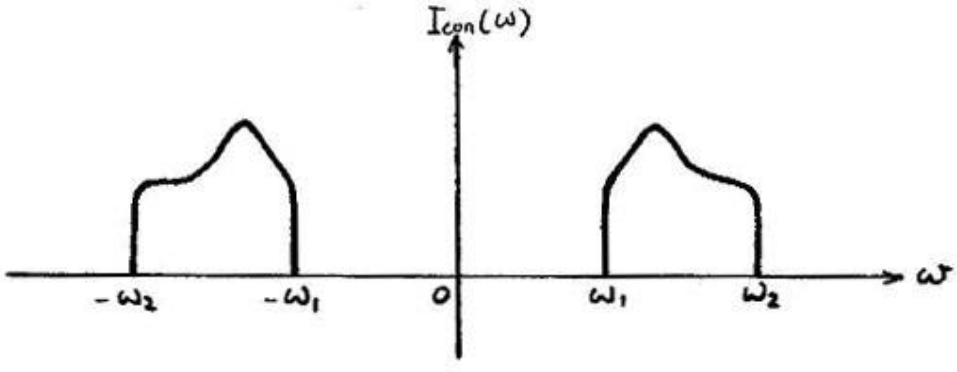

Figure 3.1(h) $I_{con}(w)$

Above is the general procedure of designing multi-beam interference given an intensity spectrum in a particular range.

If a device can provide all the T components in $\{A(T)\}$, this device can exactly construct the target spectrum:

$$I(w) - I_{con}(w) = 0, w_1 \le w \le w_2 \quad (3.14)$$

If a device cannot provide all the T components in $\{A(T)\}$, this device cannot exactly construct the target spectrum. There will be distortion:

$$I(w) - I_{con}(w) = e(w), w_1 \le w \le w_2 \quad (3.15)$$

Chapter 4 Novel Adaptive Attenuator

The reason Fabry-Perot cavities, thin-film and fiber gratings give fixed shape spectra is because the energy allocation and relative time delay allocation among the multiple beams is fixed and discrete. If a device can give arbitrary allocations of these two factors, the device can give arbitrary interference intensity spectrum to a certain extent. Based on the above idea, the novel adaptive attenuator could be realized by various technologies, such as the use of segment deformable mirrors, a liquid crystal phase modulation array, and waveguides. Adaptive equalizer is nothing but adaptive attenuator plus feedback loop.

Principles of novel adaptive attenuator are:

1. It is a multi-beam interference based device. It could generate multi-beam interference. It could arbitrarily shape the spectrum of an input light in real time.
2. It can real time arbitrarily distribute phase difference between multiple beams
3. It can real time arbitrarily distribute energy between multiple beams
4. It can distribute phase difference and energy among multiple beams individually

Theoretically, a device that could distribute arbitrary phase difference and energy among the multiple beams could realize arbitrary multi-beam interference intensity spectrum.

Technologies that can generate an incident beam are: fiber; lenses; graded-index rod lenses; prisms; etc.

Technologies that can divide an incident beam into multiple beams are: deformable mirrors; liquid crystal array; fiber coupler; Mach-Zender interferometer; waveguide; phase plate; phase stack; etc.

Technologies that can distribute phase difference $\{T\}$ among multiple beams are: deformable mirrors; liquid crystal based phase modulator; thermal modulation to the

optical index of refraction or to the geometrical distance; electro-optics modulation to the optical index of refraction; acoustic-optics modulation to the optical index of refraction; elastic-optics modulation to the optical index of refraction; birefringence caused difference to the optical index of refraction; phase plate; phase stack; etc.

Technologies that can distribute energy $\{A(T)\}$ between multiple beams are: liquid crystal based attenuator; liquide crystal based phase modulator; fiber coupler; Mach-Zender interferometer; waveguide; thermal modulation to the optical index of refraction or to the geometrical distance; electro-optics modulation to the optical index of refraction; magneto-optics modulation to the polarization state of light followed by polarizer; acoustic-optics modulation to the optical index of refraction; elastic-optics modulation to the optical index of refraction; birefringence caused difference to the optical index of refraction; phase plate; phase stack; etc.

Technologies that can combine the multiple beams are: lenses; graded-index rod lenses; prisms; waveguide couplers; fiber couplers; etc.

Combinations of these technologies can achieve novel adaptive attenuator principles. 4 examples are given below.

4.1 Liquid Crystal Phase Modulator Array based Adaptive Attenuator

This is a transmission type adaptive attenuator.

A plane wave is incident upon the liquid crystal based phase modulator array. Refractive index of each unit of the array can be controlled electronically. The light through each unit is deemed as one beam. The beams that go through the array will interfere with each other after the second focus lens. By changing the refractive index of each unit of the array so as to allocate the phase difference, we can use a computer to arbitrarily allocate $\{T\}$ among the beams. Group *k* unit into *m* groups. Among each

group, $\Delta T = 0$. $\{A(T)\}$ allocation is achieved. When the number of unit is large, energy allocation and phase allocation can be changed individually.

The system deployment is plotted in Figure 4.1.

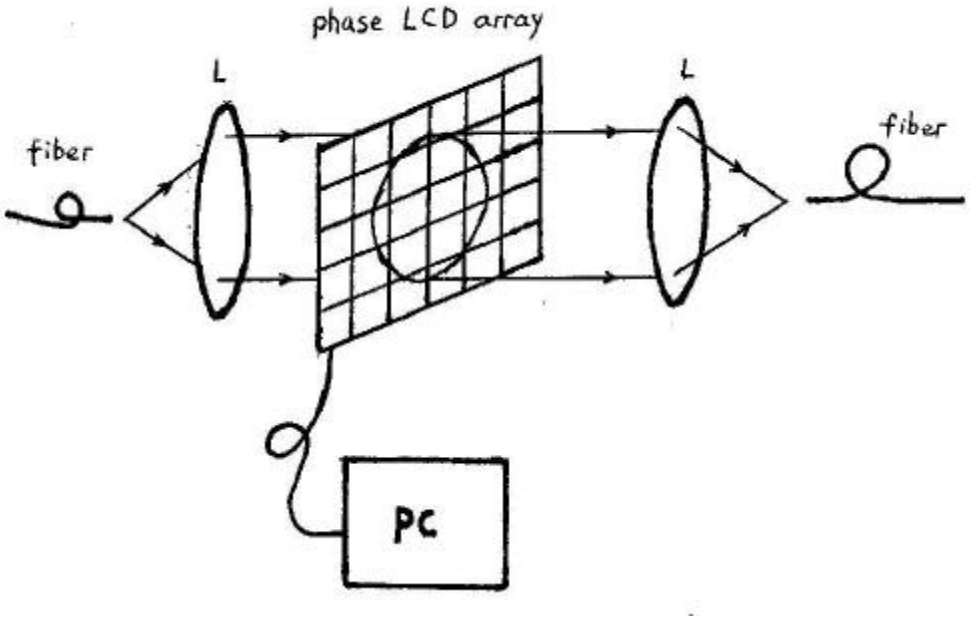

Figure 4.1 Phase-LCD array based adaptive attenuator

4.2 Mach-Zender Interferometer based Adaptive Attenuator

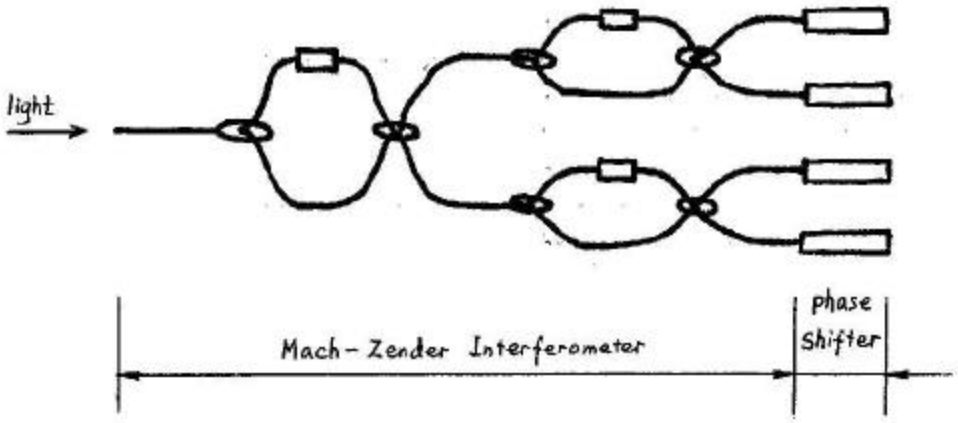

Figure 4.2 Mach-Zender interferometer based adaptive attenuator

Light comes in at the input of Mach-Zender interferometer. Phase of one arm of the interferometer can be changed so as to arbitrarily allocate the energy between the two

output ports. By repeating the same unit interferometer, one beam can be split into multiple beams. These beams will interfere with each other when focused. We can use phase shifter to arbitrarily allocate $\{T\}$ among the beams. Group *k* beams into *m* groups. Among each group, $\Delta T = 0$. $\{A(T)\}$ allocation is achieved. When the number of unit is large, energy allocation and phase allocation can be changed individually.

4.3 Phase Mask based Adaptive Attenuator

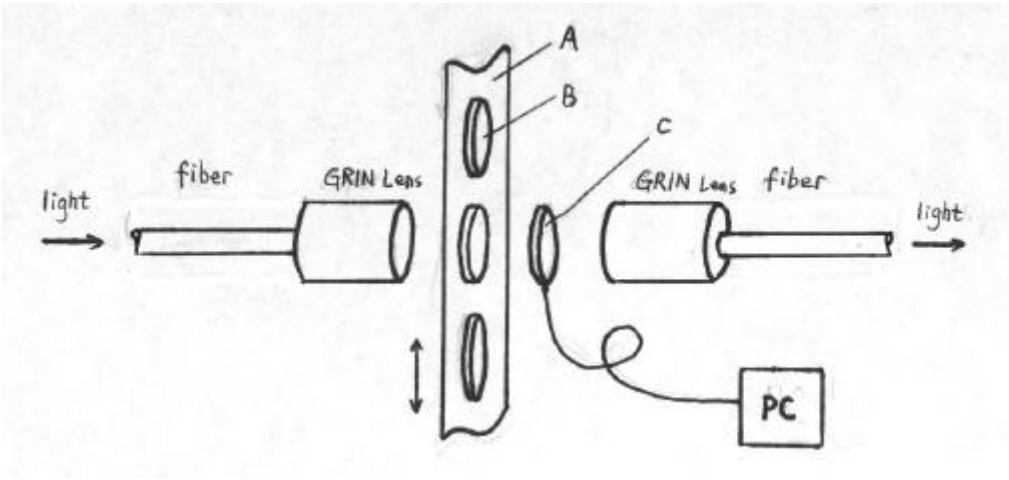

Figure 4.3 Phase mask based adaptive attenuator

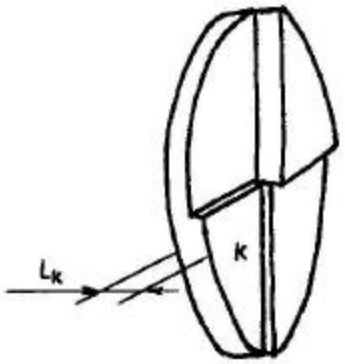

Figure 4.4(a) Structure of phase mask

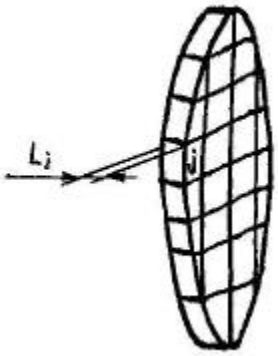

Figure 4.4(b) structure of phase shifter

After the GRIN (Graded Index Fiber) lens, the light can be deemed as a plane wave. The light goes through phase mask B and phase modulator C, collected by GRIN lens and transmitted by fiber. The system deployment is shown in Figure 4.3.

Structure of phase mask and phase modulator is shown in Figure 4.4. Phase mask divides the plane wave into multiple beams with different relative light path difference. A phase mask is designed to give a particular interference spectrum. By putting a group of different phase masks on a plate A and move A, we can allocate different sets of $\{T\}$ among the beams. The function of the phase shifter C is to modulate the $\{T\}$ in a small scale after the phase mask B. Thus arbitrary $\{T\}$ is realized. Group k beams into m groups. Among each group, $\Delta T = 0$. $\{A(T)\}$ allocation is achieved. When the number of beams is large, energy allocation and phase allocation can be changed individually.

4.4 Phase Modulation Stack based Adaptive Attenuator

After the GRIN (Graded Index Fiber) lens, the light can be deemed as a plane wave. The light goes through phase modulation stack A, collected by GRIN lens and transmitted by fiber as shown in Figure 4.5.

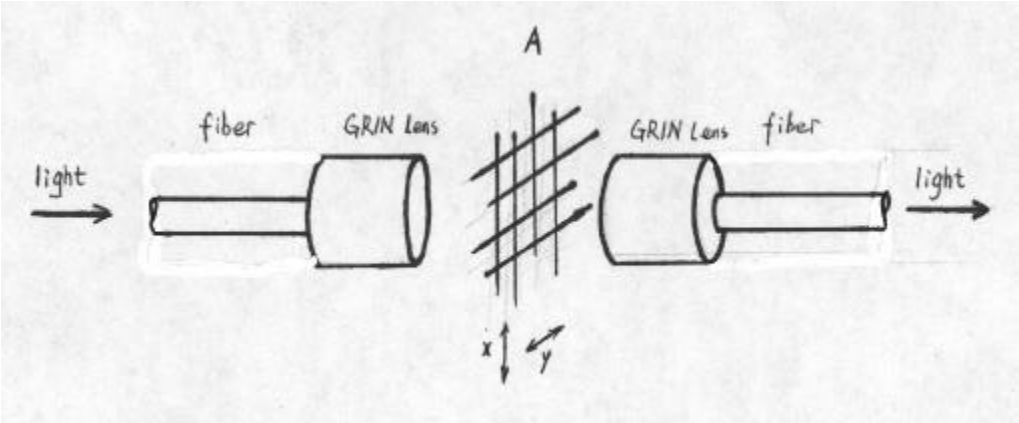

Figure 4.5 Phase modulation stack based adaptive attenuator

Structure of phase modulation stack and the unit structure of phase modulation stack are shown in Figure 4.6. Phase modulation stack divides the plane wave into multiple beams with different relative light path difference. The unit of the phase modulation stack is composed of segments of different refractive index. Align the units in X and Y directions form the phase modulation stack. Each unit is movable. Different combinations of each unit position will give different sets of $\{T\}$. Group k beams into m groups. Among each group, $\Delta T = 0$. $\{A(T)\}$ allocation is achieved. When the number of beams is large, energy allocation and phase allocation can be changed individually.

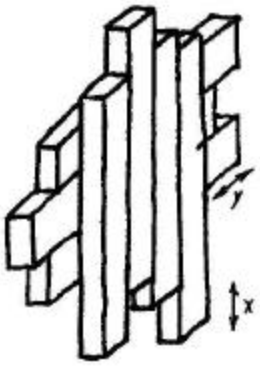

Figure 4.6(a) Structure of phase modulation stack

Figure 4.6(b) Unit structure of phase modulation stack

Chapter 5 Segment Deformable Mirror based Adaptive Attenuator

5.1 Device Principles and Configuration

Segment Deformable Mirror (SDM) is an array of micro mirrors made on a back plane. The vertical position of each mirror can be precisely controlled by an array of micro-machined driver (heart of the driver is usually based on piezoelectric elements). Figure 5.1 gives the outlook of segment deformable mirror and actuators. Figure 5.2 illustrates the basic unit of deformable mirror.

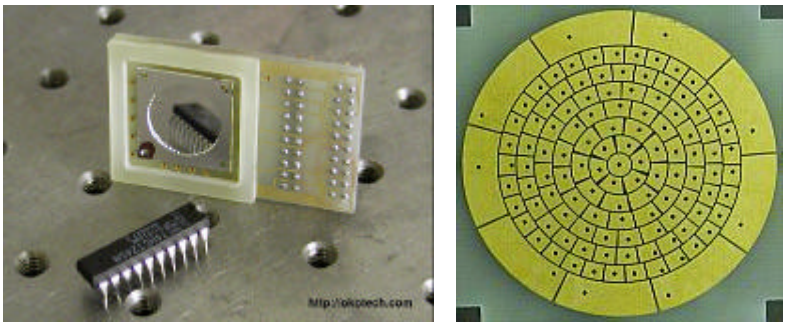

Figure 5.1 Outlook of deformable mirror and actuators

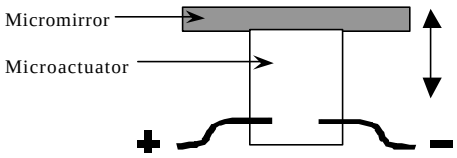

Figure 5.2 Basic unit of deformable mirror

Assume a plane wave of monochromatic light is incident upon deformable mirror at angle q . The light reflected from each mirror can be deemed as one beam. All the light in one beam has the same deformable mirror introduced relative delay and the same magnitude.

Suppose deformable mirror has *k* unit reflection mirrors, and then *k*-beam interference could be achieved. Adaptive attenuator principle 1 is realized.

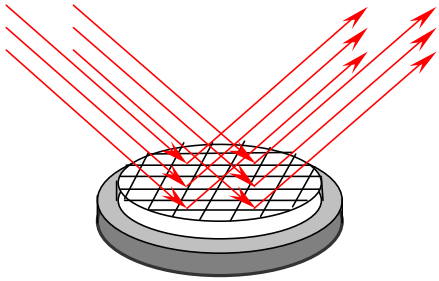

Figure 5.3 Deformable mirror as multi-beam interference device

Assume a plane wave of monochromatic light is incident upon deformable mirror at angle q. M_1 and M_2 are two unit reflection mirrors of deformable mirror (they are not necessarily adjacent). The vertical difference of these two mirrors is $\Delta L = L_1 - L_2$. This would result in the phase difference of Beam 1 and Beam 2. The relative phase difference is given as $d_{1,2} = \frac{4p}{l}\Delta L\cos q$, which is a linear function of ΔL, and inversely proportional to l. Let $d_{1,2} = \frac{4p}{l}\Delta L\cos q = w L, w = 2p f$, and $\Delta T = \frac{2\Delta L\cos q}{c}$. So if we change ΔL among the *k* unit reflection mirrors, we can distribute relative delay $\{T\}$ among *k* reflected beams. Thus adaptive attenuator principle 2 is realized.

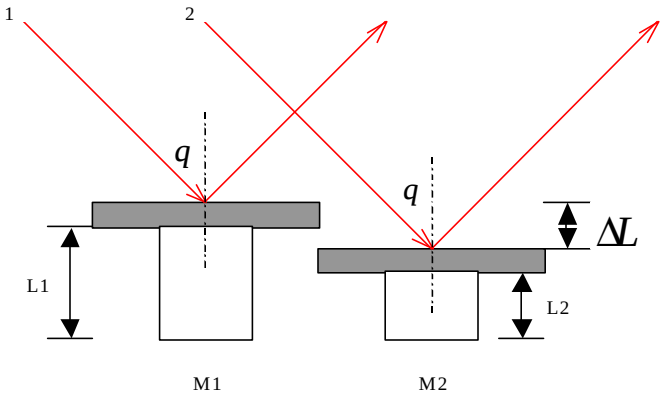

Figure 5.4 Deformable mirror as phase modulation device

Assume a plane wave of monochromatic light is incident upon DM at angle q. M_1, M_2 and M_3 are three unit reflection mirrors of DM (they are not necessarily adjacent) as shown in Figure 5.5. The vertical difference of these two mirrors is $\Delta L_{1,2} = 0, \Delta L_{1,3} = \Delta L_{2,3} = L_1 - L_3$. Since $\Delta L_{1,2} = 0$, beam 1 and beam 2 have no phase difference. Assume beam 1 and beam 2 have equal complex amplitude ae^{-jd}, and then these two beams can be taken as one beam with complex amplitude as $2ae^{-jd}$. Thus $A(T_1) : A(T_3) = 2:1$. So if we group *k* unit reflection mirrors into *m* groups. Among each group, $\Delta T = 0$. Energy distribution $\{A(T)\}$ is achieved. Adaptive attenuator principle 3 is realized.

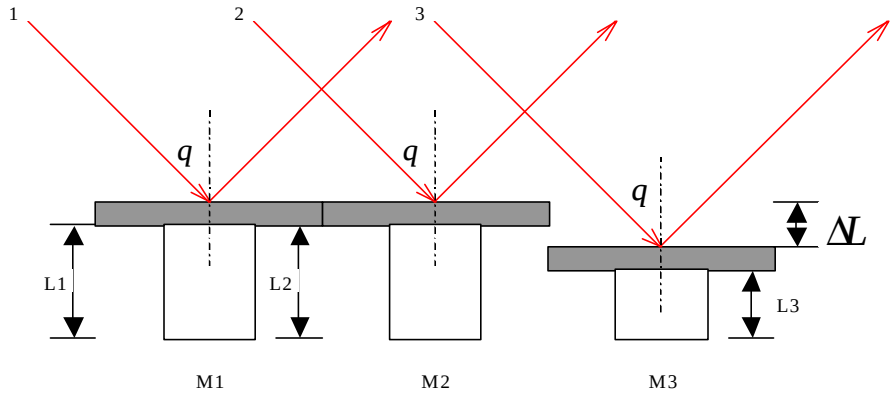

Figure 5.5 Deformable mirror as magnitude modulation device

The structure of deformable mirror based adaptive equalizer is illustrated in Figure 5.6.

Light is emitted from fiber S carrying WDM channels. When it goes through lens L, it becomes plane wave. The wavefront is plane, as denoted by W in Figure 5.6. The incident plane wave is reflected from Deformable Mirrors, which is controlled by computer. DM completes energy allocation and phase allocation among the multi beams. The modulated wavefront is denoted as W' in Figure 5.6. The reflected light is collected by lens L', and forms multi-beam interference on plane P. By positioning a

collecting fiber at the ideal focal point on plane P, the WDM channels after equalization is collected and transmitted by this fiber. A coupler is used to monitor the spectrum after equalization and feed information back to the computer.

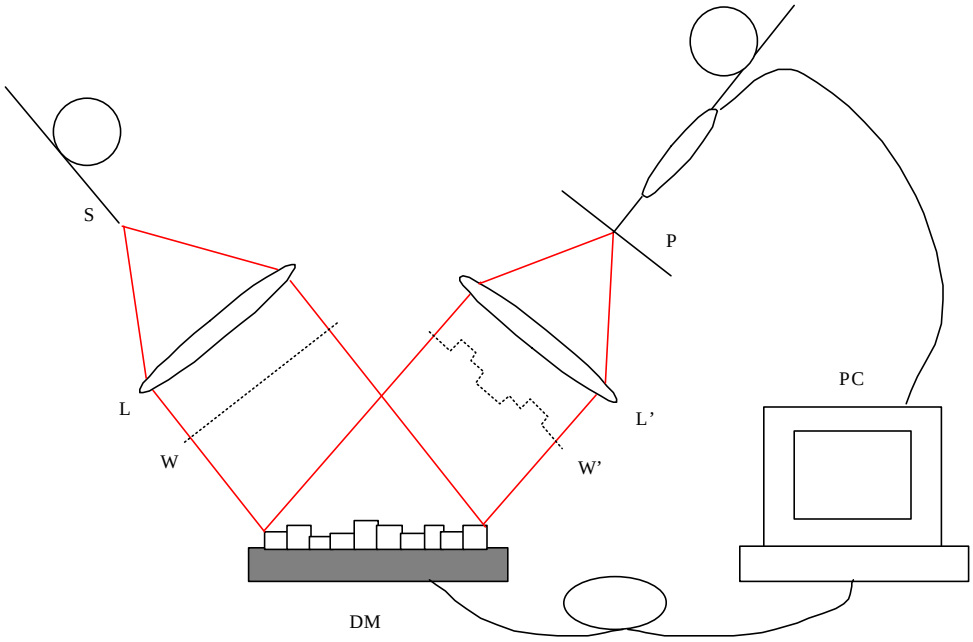

Figure 5.6 Structure of deformable mirror based adaptive equalizer

When the number of unit micro mirrors is large, energy allocation and phase allocation can be changed individually. Thus adaptive attenuator principle 4 is realized.

By controlling the deformation mirrors, the computer can real-time shape the spectrum. Since adaptive equalizer system is reflection based, we can apply a thin-gold-film on DM, the energy reflection coefficient R can almost be 1. This will result in very small insertion loss of the system.

5.2 Realization of Real $\{E(w)\}$ and Negative $\{A(T)\}$

According to the principles of spectrum design, the one way to have real $\{A(T)\}$ is to have real and even $\{E(w)\}$. Real and even $\{E(w)\}$ forces $\{A(T)\}$ to be real and even.

For deformable mirrors, real and even $\{A(T)\}$ means all the mirrors should be symmetrically distributed to the zero phase mirrors as illustrated in Figure 5.7.

To realize negative $A(T_i)$, the mirrors of $\pm L_i$ should move a certain distance so as to add an additional phase shift of p. To keep the symmetric distribution, the mirrors of $+L$ should move opposite to the mirrors of $-L$ as illustrated in Figure 5.8.

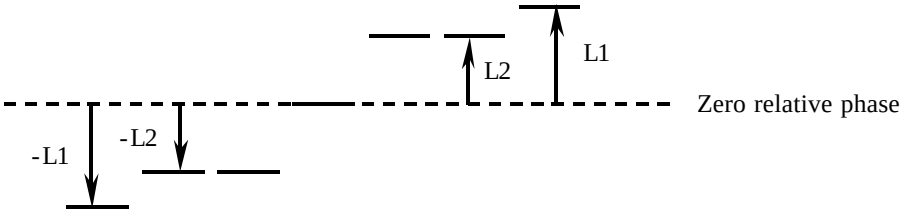

Figure 5.7 symmetrically distributed mirrors

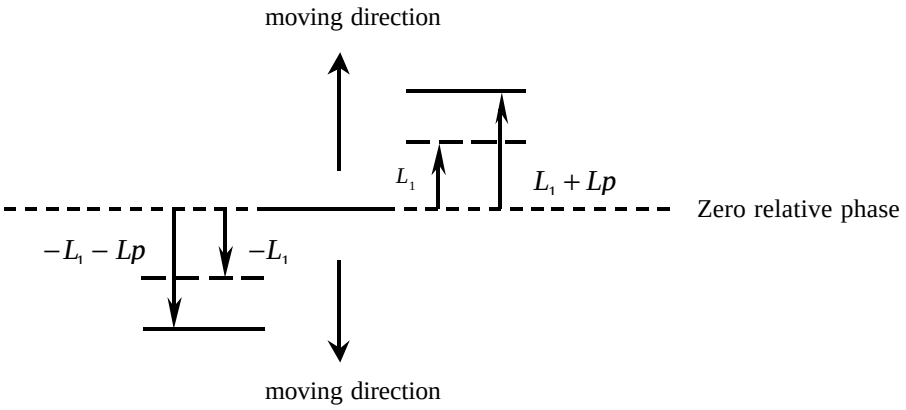

Figure 5.8(a) Realize of negative $A(T)$

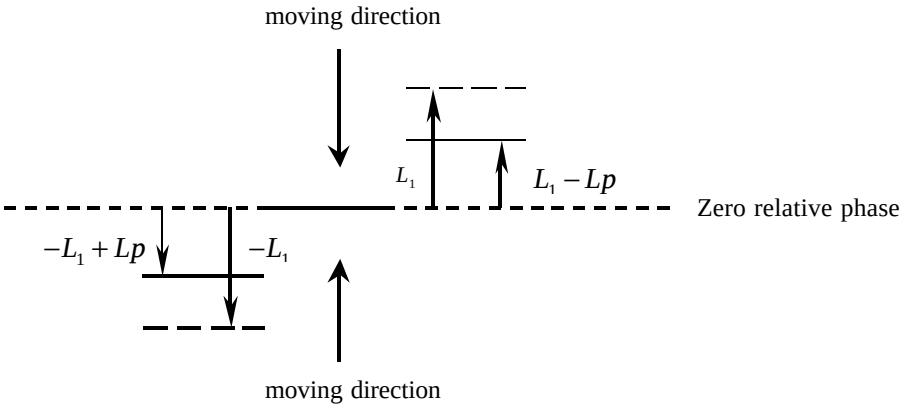

Figure 5.8(b) Realize of negative $A(T)$

5.3 Alternative Explanation of Variable Transmisitivity

Adaptive attenuator has variable transmisitivity, which can be explained using interference theory. Consider a two-slot interference experiment shown in Figure 5.9. Plane and coherent wave with wavelength l is incident on the slots. Both slot S_1 and S_2 can be deemed as coherent light sources. The light is collected by the lens and generate interference pattern on the focal plane P. When light path for both light

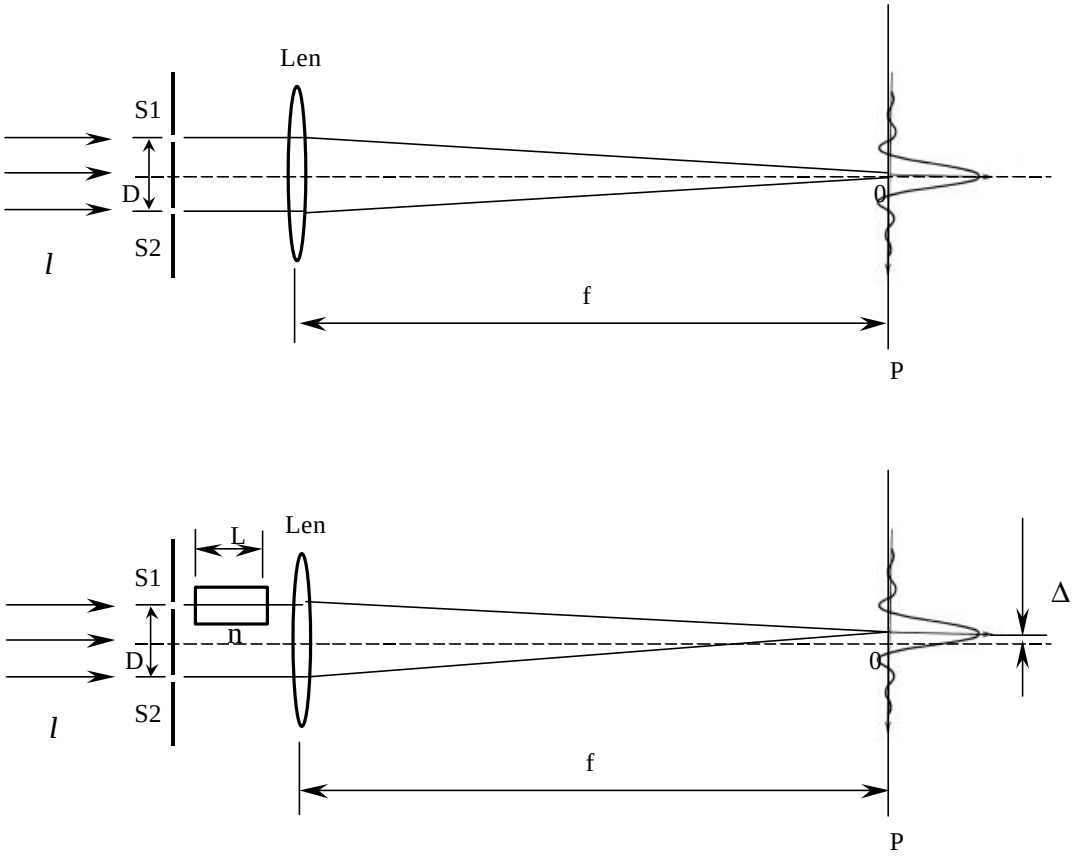

Figure 5.9 Two-slot interference experiment

sources is the same, the zero order interference pattern occurs at $x = 0$. When a piece of glass with refractive index of n and length of L is inserted into the ray path of source S_1, the zero order interference pattern moved to $\Delta(L) = \frac{(n-1)Lf_0}{D}$, when D and f_0 are fixed. The intensity at $x = 0$ is proportional to $\cos[\frac{2p(n-1)L}{l}]$, in other words, the

intensity at the point $x = 0$ is modulated by l and L. When a fiber is placed at this point, the transmisitivity of l can thus be adaptively attenuated. And this is the principle of the adaptive attenuator.

5.4 Discrete Relative Delay Spectrum Design

For an actual digitally controlled adaptive attenuator, there are fundamental limits for device performance. They are: relative delay range $|\Delta T|_{\max}$, number of bits of control b and number of mirrors N. Since the relative delay components $\{\Delta T\}$ the device can provide is discrete and limited, the methodology developed in Chapter 3 is no longer suitable. The theory of attenuation spectrum design based on discrete relative delay spectrum is discussed below.

From *Fourier transform* theory we know that a discrete periodic time signal $x(nT_s)$ has discrete periodic spectrum $X(kf_1)$ as shown in Figure 5.10

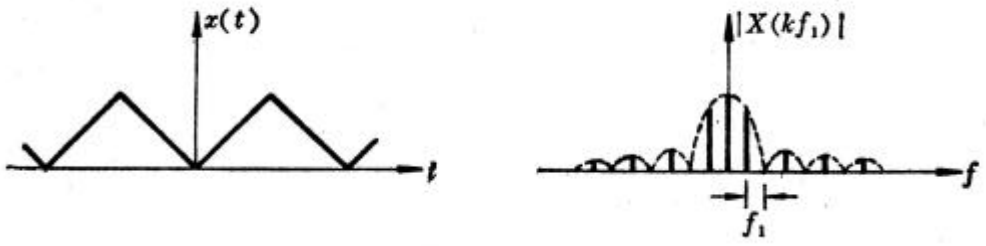

Figure 5.10 Time signal and its spectrum

where $f_1 = 1/T_1$, and T_1 is t he period of the time varying signal: $x(t + T_1) = x(t)$.

It is the same in the optical spectrum and relative delay spectrum as shown in Figure 5.11.

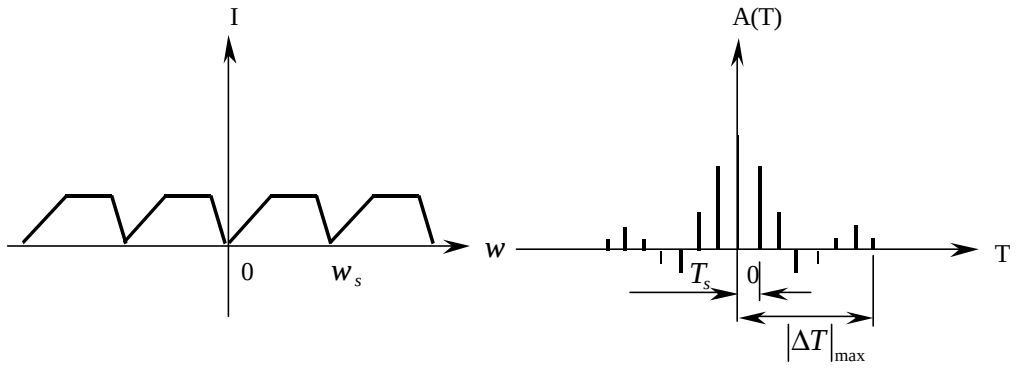

Figure 5.11 optical spectrum and its relative delay spectrum

where $T_s = 2p/w_s = |\Delta T|_{\max}/2^{b-1}$.

The step of spectrum design for the deformable mirror based adaptive attenuator is:

1. Calculate the quantization step $T_s = |\Delta T|_{\max}/2^{b-1}$, where

$|\Delta T|_{\max} = \dfrac{2\cos q\, \Delta L_{\max}/2}{c}$, $\Delta L_{\max}$ is the maximum vertical movable range that the deformable mirror can cover.

2. Calculate $w_s = 2p/T_s$

3. Expand the desired attenuation spectrum $I(w)$ with period w_s and get $I_p(w)$

4. Fourier transform of $I_p(w)$ gives discrete spectrum components that the device can provide.

5.5 Simulation Results for SDM based Adaptive Attenuator Performance

Simulation results of the impact of relative delay range $|\Delta T|_{\max}$, number of bits of control b and number of mirrors N are given in Figure 5.12. The simulation results are obtained in the following way:

1. Randomly generate a normalized function $I(x)$

2. Denote square root of $I(x)$ as $E(x)$
3. Denote discrete cosine transform of $E(x)$ as $A(T)$
4. Assume 15^0 incident angle
5. In Spectrum vs. Bits and Spectrum vs. L Range, quantize T using quantizer $\frac{L/2}{2^b}$, b is the number of bits, L is the total dynamic range of the mirror, $L/2$ is the effective dynamic range of the mirror; inverse DTC (Discrete Cosine Transform) gives new $E(x)$, and $I(x)$ is the square of $E(x)$
6. In Spectrum vs. Number of Mirror, quantize $\frac{A(T)}{\Sigma A(T)}$ using quantizer $\frac{1}{N}$, N is the number of the mirror. The result is recorded as a new $A(T)$. Use the new $A(T)$ to construct the inverse DTC gives new $E(x)$, and $I(x)$ is the square of $E(x)$. Normalize $I(x)$ gives the result.

The results indicate that segment deformable mirror of 10bits, 3200 elements and total phase range of $10mm$ can give a good approximation of such target spectrum.

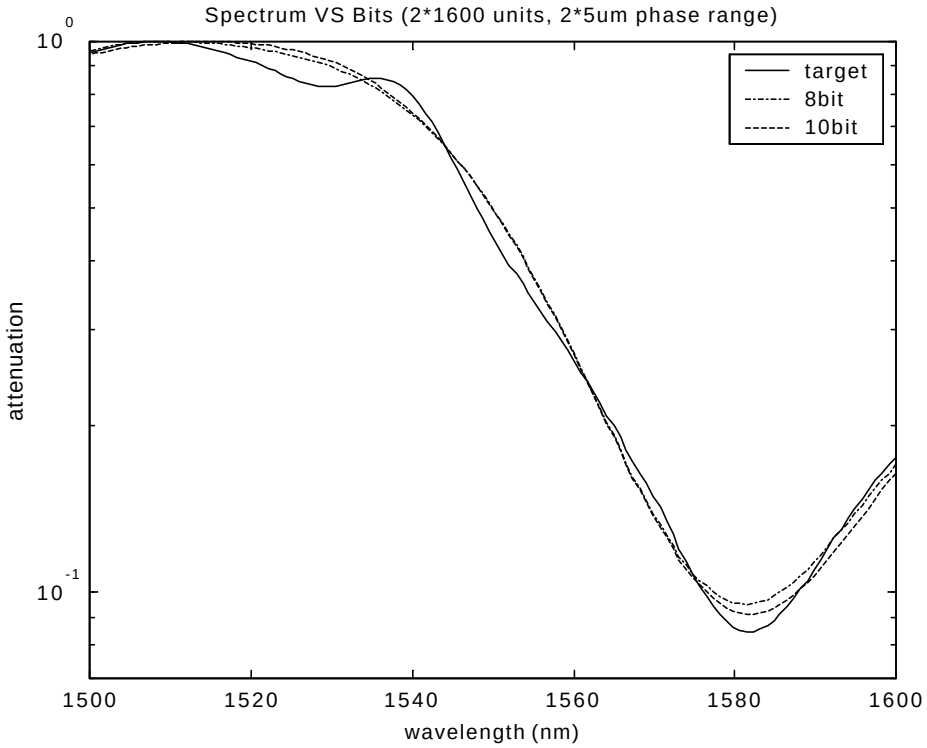
Spectrum VS Bits (2*1600 units, 2*5um phase range)
10^0
10^-1
attenuation
target
8bit
10bit
1500
1520
1540
1560
1580
1600
wavelength (nm)

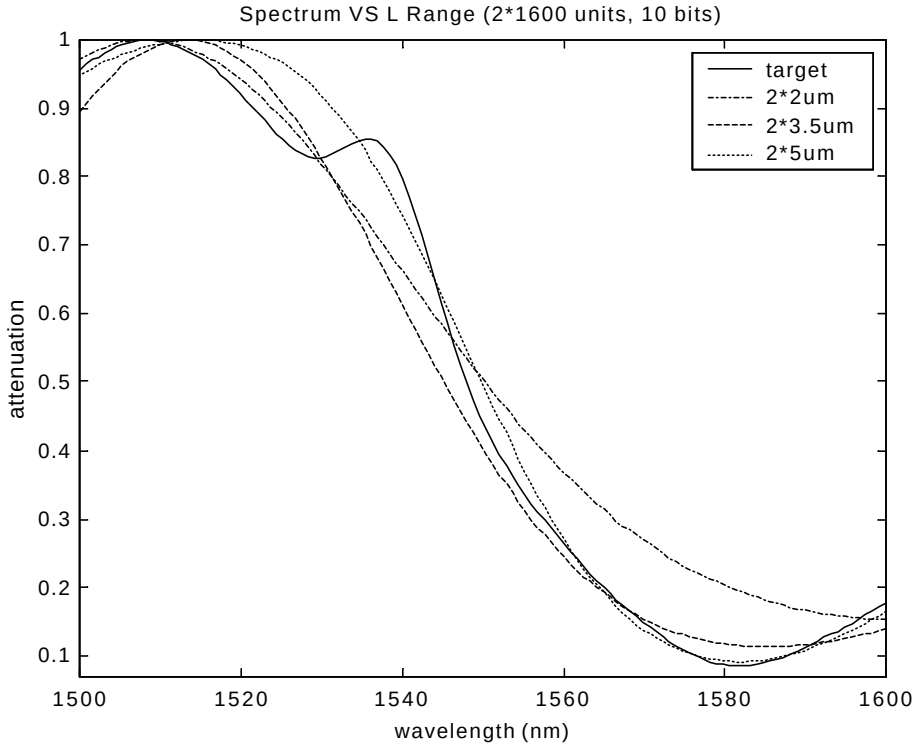
Spectrum VS L Range (2*1600 units, 10 bits)
1
0.9
0.8
0.7
0.6
0.5
0.4
0.3
0.2
0.1
attenuation
target
2*2um
2*3.5um
2*5um
1500
1520
1540
1560
1580
1600
wavelength (nm)

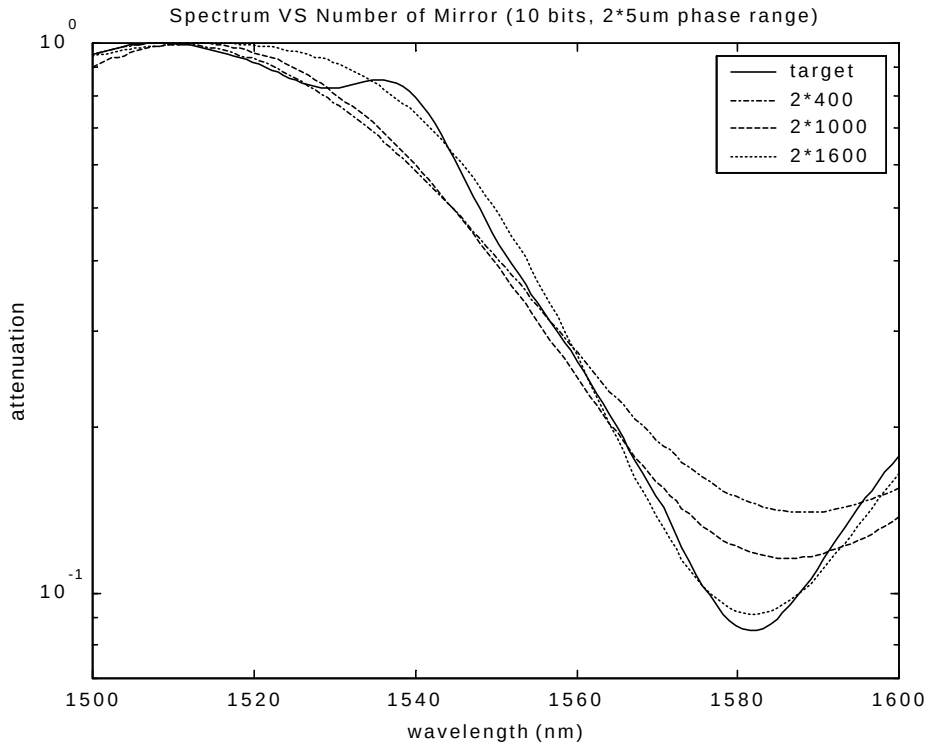

Figure 5.12 Simulation results of segment deformable mirror based adaptive attenuator performance

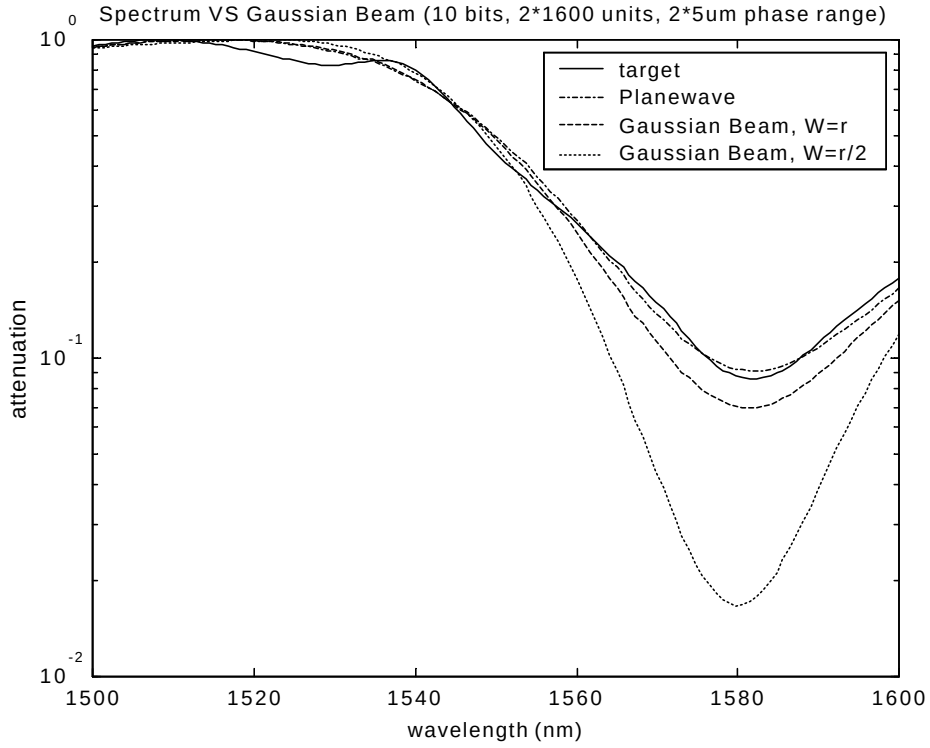

Figure 5.13 Simulation results of segment deformable mirror based adaptive attenuator performance

In the previous analysis, plane incident wave is assumed. However, in real application, gaussian beam assumption is more applicable. Figure 5.13 showed the simulation results. A gaussian beam is incident on the round deformable mirror and reflected. Two situations are calculated.

Chapter 6 Conclusion and Future Work

In this thesis, Fourier analysis of multi-beam interference is first proposed, and then applied for multi-beam interference design. Several novel adaptive attenuators based on the idea of Fourier analysis are presented. The adaptive attenuator based on segment deformable mirror is studied in detail, and its performance simulation result is given.

Fourier analysis is a very powerful tool in multi-beam interference device analysis and design. Devices with high efficiency can be designed based on this understanding. Segment deformable mirror based adaptive attenuator is one of the best realizations of the above idea. It is a powerful tool to shape the spectrum. It has great advantages over traditional multi-beam interference device such as: real-time arbitrary spectrum shaping; low insertion loss; high speed; computer controlled; polarization insensitive; simple device structure; high flexibility. Its disadvantage might be: the performance is relevant to the accuracy of the lens system; the performance is relevant to the position accuracy, numerical aperture and diameter of the core of the collecting fiber; the device performance is sensitive with segment mirror phase control accuracy and the energy distribution of the beam, etc.

The future work involves further simulation of lens aberration introduced effect, collecting fiber position and aperture introduced effect, segment mirror phase control tolerance introduced effect. And also work will be done on the compensation issue such as pre-weight of mirrors to eliminate gaussian beam introduced performance degradation, etc.

Reference

[1] Govind P. Agrawal, Fiber –Optic Communication Systems, 2nd edition, John Wiley & Sons, Inc, 1997

[2] Doerr, C.R; Schiffer, P; Stulz, L.W; Cappuzzo, M; Laskowski, E; Paunescu, A; Gomez, L; Gates, J; "Compact Integrated Dynamic Wavelength Equalizer" Optical Fiber Communication Conference, 1999, and the International Conference on Integrated Optics and Optical Fiber Communication. OFC/IOOC '99. Technical Digest, 1999. PD30/1 -PD30/3 Suppl.

[3] Riza; Nabeel Agha; "Fault-tolerant fiber-optical beam control modules", United States Patent 6,222,954, April 24, 2001.

[4] Aksyuk; Vladimir A; Barber; Bradley P; Bishop; David .J; Giles; Clinton R; Stulz; Lawrence W; Ruel; Rene R; "Optical *attenuator*", United States Patent 6,173,105, January 9, 2001.

[5] Bergmann; Ernest Eisenhardt; Bishop; David John; "Micro-mechanical variable optical attenuator", United States Patent 6,163,643, December 19, 2000.

[6] Abbott; Robert Ralph; Berkstresser; George Wayne; Brandle, Jr.; Charles David; Fratello; Vincent Jerome; Licht; Steven Joy; "Article comprising a variable optical *attenuator*", United States Patent 5,978,135, November 2, 1999.

[7] S. H. Huang; X. Y. Zou; S. M. Hwang; A. E. Willner; Z. Bao, and D. A. Smith; "Experimental demonstration of dynamic network equalization of three 2.5 Gb/s WDM channels over 1000 km using acoustooptic tunable fiters", IEEE Photonics. Technology. Lett., vol. 8, pp. 1243-1245, 1996

[8] H. S. Kim; S. H. Yun; H. K. Kim; N. Park and B. Y. Kim, "Actively gain-flatterned erbium-doped fiber amplifier over 35nm by using all-fiber acoustooptic tunable filters", IEEE Photonics Technology Lett., vol. 10, pp. 790-792, 1998.

[9] K. Inoue; T. Kominato and H. Toba; “Tunable gain equalization using a Mach-Zehnder optical filter in multistage fiber amplifiers”, IEEE Photonics Technology Lett., vol. 3, pp. 718-720, 1991.

[10] M. Zirngibl; C. H. Joyner and B. Glance, “Digitally tunable channel dropping filter/equalizer based on waveguide grating router and optical amplifier integration”, IEEE Photonics Technology Lett., vol. 6, pp. 513-515, 1994.

[11] C. R. Doerr; C. H. Joyner and L. W. Stulz; “Integrated WDM dynamic power equalizer with potentially low insertion loss”, IEEE Photonics Technology Lett., vol. 10, pp. 1443-1445, 1998.

[12] M. C. Parker; A. D. Cohen and R. J. Mears; “Dynamic holographic spectral equalization for WDM”, IEEE Photonics Technology Lett., vol. 9, pp. 529-531, 1997.

[13] Ford, J.E.; Walker, J.A, Broadband Optical Networks and Technologies: An Emerging Reality/Optical MEMS/Smart Pixels/Organic Optics and Optoelectronics. 1998 IEEE/LEOS Summer Topical Meetin , 1998, pp I/9 -I10

[14] Offrein, B.J.; Bona, G.L.; Germann, R.; Horst, F.; Salemink, H.W.M, LEOS '99. IEEE Lasers and Electro-Optics Society 1999 12th Annual Meeting , Volume: 2 , 1999, pp 547 -548 vol.2

[15] Doerr, C.R.; Joyner, C.H.; Stulz, L.W, IEEE Photonics Technology Letters , Volume: 10 Issue: 10 , Oct. 1998, pp 1443 -1445

[16] Mansell, Justin Dennis, “Micromachined Deformable Mirrors for Laser Wavefront Control”, PhD thesis, Electrical Engineering Department, Stanford University, Feb, 2002, Chapter 4

[17] T. G. Bifano, J. Perreault, R. Krishnamoorthy Mali, and M. N. Horenstein. "Microelectromechanical Deformable Mirrors", IEEE J. of Sel. Top. In Quan. Elec. **5**, 83-9, 1999.

[18] M. A. Michalicek, N. Clark, J. H. Comtois, and H. K. Schriner. "Design and simulation of advanced surface micromachined micromirror devices for telescope adaptive optics applications", SPIE Vol. 3353, 805-815, 1998.

Appendix A Matlab Program for Spectrum vs. Bits

```
clear all;
%%%%%%%%%%%%%%%%%%%%%% generate target spectrum %%%%%%%%%%%%%%%%%%%%%%
angle=cos((15/180)*pi);
limit1=round((1e12*(2*angle*(5e-6/2^7)./3e8))^-1);
freq=1:limit1;
I_semi_target1=10*exp(-(freq-1990).^2/2000)+3*exp(-(freq-
1950).^2/100)+4*exp(-abs(freq-1910)./300)-3*exp(-abs(freq-
1900).^2/800);
I_target1=0.01+0.99*((I_semi_target1-
min(I_semi_target1))/(max(I_semi_target1)-min(I_semi_target1)));
E1=sqrt(I_target1);
%%%%%%%%%%%%%%%%%%%%%% get the wavelets %%%%%%%%%%%%%%%%%%%%%%%%%%%%
b_r1=(dct(E1));
b_r1(129:limit1)=0;
b_r_sum1=sum(abs(b_r1));
b1=round(b_r1/(0.000625*b_r_sum1))*(0.000625*b_r_sum1);
E_rec1=(idct(b1));
I_rec1=E_rec1.^2;
I_max1=max(I_rec1);
I_rec_1=I_rec1/I_max1;
%%%%%%%%%%%%%%%%%%%%%% generate target spectrum %%%%%%%%%%%%%%%%%%%%%%
angle=cos((15/180)*pi);
limit2=round((1e12*(2*angle*(5e-6/2^9)./3e8))^-1);
freq=1:limit2;
I_semi_target2=10*exp(-(freq-1990).^2/2000)+3*exp(-(freq-
1950).^2/100)+4*exp(-abs(freq-1910)./300)-3*exp(-abs(freq-
1900).^2/800);
I_target2=0.01+0.99*((I_semi_target2-
min(I_semi_target2))/(max(I_semi_target2)-min(I_semi_target2)));
```

```
E2=sqrt(I_target2);
%%%%%%%%%%%%%%%%%%%%%% get the wavelets %%%%%%%%%%%%%%%%%%%%%%%%%%%%
b_r2=(dct(E2));
b_r2(513:limit2)=0;
b_r_sum2=sum(abs(b_r2));
b2=round(b_r2/(0.000625*b_r_sum2))*(0.000625*b_r_sum2);
E_rec2=(idct(b2));
I_rec2=E_rec2.^2;
I_max2=max(I_rec2);
I_rec_2=I_rec2/I_max2;
%%%%%%%%%%%%%%%%%%%%%%%%%%%%%%%%%%%%%%%%%%%%%%%%%%%%%%%%%%%%%%%%%%%%%%%
ii=1875:2000;
figure;semilogy(3e6./ii,I_target1(ii),'k',3e6./ii,I_rec_1(ii),'k-
.',3e6./ii,I_rec_2(ii),'k--');
axis([1.5e3 1.6e3 0.7e-1 1]);
xlabel('wavelength (nm)');ylabel('attenuation');title('Spectrum VS
Bits (2*1600 units, 2*5um phase range)');
legend('target','8bit','10bit');
```

Appendix B Matlab Program for Spectrum vs. Phase Range

```
clear all;
%%%%%%%%%%%%%%%%%%%%%% generate target spectrum %%%%%%%%%%%%%%%%%%%%%%
angle=cos((15/180)*pi);
limit1=round((1e12*(2*angle*(2e-6/2^9)./3e8))^-1);
freq=1:limit1;
I_semi_target1=10*exp(-(freq-1990).^2/2000)+3*exp(-(freq-
1950).^2/100)+4*exp(-abs(freq-1910)./300)-3*exp(-abs(freq-
1900).^2/800);
I_target1=0.01+0.99*((I_semi_target1-
min(I_semi_target1))/(max(I_semi_target1)-min(I_semi_target1)));
E1=sqrt(I_target1);
%%%%%%%%%%%%%%%%%%%%%% get the wavelets %%%%%%%%%%%%%%%%%%%%%%%%%%%%
b_r1=(dct(E1));
b_r1(513:limit1)=0;
b_r_sum1=sum(abs(b_r1));
b1=round(b_r1/(0.000625*b_r_sum1))*(0.000625*b_r_sum1);
E_rec1=(idct(b1));
I_rec1=E_rec1.^2;
I_max1=max(I_rec1);
I_rec_1=I_rec1/I_max1;
%%%%%%%%%%%%%%%%%%%%%% generate target spectrum %%%%%%%%%%%%%%%%%%%%%%
angle=cos((15/180)*pi);
limit2=round((1e12*(2*angle*(3.5e-6/2^9)./3e8))^-1);
freq=1:limit2;
I_semi_target2=10*exp(-(freq-1990).^2/2000)+3*exp(-(freq-
1950).^2/100)+4*exp(-abs(freq-1910)./300)-3*exp(-abs(freq-
1900).^2/800);
I_target2=0.01+0.99*((I_semi_target2-
min(I_semi_target2))/(max(I_semi_target2)-min(I_semi_target2)));
```

```
E2=sqrt(I_target2);
%%%%%%%%%%%%%%%%%%%%% get the wavelets %%%%%%%%%%%%%%%%%%%%%%%%%%%%
b_r2=(dct(E2));
b_r2(513:limit2)=0;
b_r_sum2=sum(abs(b_r2));
b2=round(b_r2/(0.000625*b_r_sum2))*(0.000625*b_r_sum2);
E_rec2=(idct(b2));
I_rec2=E_rec2.^2;
I_max2=max(I_rec2);
I_rec_2=I_rec2/I_max2;
%%%%%%%%%%%%%%%%%%%%% generate target spectrum %%%%%%%%%%%%%%%%%%%%%
angle=cos((15/180)*pi);
limit3=round((1e12*(2*angle*(5e-6/2^9)./3e8))^-1);
freq=1:limit3;
I_semi_target3=10*exp(-(freq-1990).^2/2000)+3*exp(-(freq-
1950).^2/100)+4*exp(-abs(freq-1910)./300)-3*exp(-abs(freq-
1900).^2/800);
I_target3=0.01+0.99*((I_semi_target3-
min(I_semi_target3))/(max(I_semi_target3)-min(I_semi_target3)));
E3=sqrt(I_target3);
%%%%%%%%%%%%%%%%%%%%% get the wavelets %%%%%%%%%%%%%%%%%%%%%%%%%%%%
b_r3=(dct(E3));
b_r3(513:limit3)=0;
b_r_sum3=sum(abs(b_r3));
b3=round(b_r3/(0.000625*b_r_sum3))*(0.000625*b_r_sum3);
E_rec3=(idct(b3));
I_rec3=E_rec3.^2;
I_max3=max(I_rec3);
I_rec_3=I_rec3/I_max3;
%%%%%%%%%%%%%%%%%%%%%%%%%%%%%%%%%%%%%%%%%%%%%%%%%%%%%%%%%%%%%%%%%%%%%%
ii=1875:2000;
```

```
figure;plot(3e6./ii,I_target1(ii),'k',3e6./ii,I_rec_1(ii),'k-
.',3e6./ii,I_rec_2(ii),'k--',3e6./ii,I_rec_3(ii),'k:');
axis([1.5e3 1.6e3 0.7e-1 1]);
xlabel('wavelength (nm)');ylabel('attenuation');title('Spectrum VS L
Range (2*1600 units, 10 bits)');
legend('target','2*2um','2*3.5um','2*5um');
iii=1:5000;
figure;semilogy(iii,I_target1(iii));

save eugene_final1.mat
```

Appendix C Matlab Program for Spectrum vs. Mirror Number

```
clear all;
%%%%%%%%%%%%%%%%%%%%%% generate target spectrum %%%%%%%%%%%%%%%%%%%%%%
angle=cos((15/180)*pi);
limit1=round((1e12*(2*angle*(5e-6/2^9)./3e8))^-1);
freq=1:limit1;
I_semi_target1=10*exp(-(freq-1990).^2/2000)+3*exp(-(freq-
1950).^2/100)+4*exp(-abs(freq-1910)./300)-3*exp(-abs(freq-
1900).^2/800);
I_target1=0.01+0.99*((I_semi_target1-
min(I_semi_target1))/(max(I_semi_target1)-min(I_semi_target1)));
E1=sqrt(I_target1);
%%%%%%%%%%%%%%%%%%%%%% get the wavelets %%%%%%%%%%%%%%%%%%%%%%%%%%%%
b_r1=(dct(E1));
b_r1(513:limit1)=0;
b_r_sum1=sum(abs(b_r1));
b1=round(b_r1/(b_r_sum1/400))*(b_r_sum1/400);
E_rec1=(idct(b1));
I_rec1=E_rec1.^2;
I_max1=max(I_rec1);
I_rec_1=I_rec1/I_max1;
%%%%%%%%%%%%%%%%%%%%%% generate target spectrum %%%%%%%%%%%%%%%%%%%%%%
angle=cos((15/180)*pi);
limit2=round((1e12*(2*angle*(5e-6/2^9)./3e8))^-1);
freq=1:limit2;
I_semi_target2=10*exp(-(freq-1990).^2/2000)+3*exp(-(freq-
1950).^2/100)+4*exp(-abs(freq-1910)./300)-3*exp(-abs(freq-
1900).^2/800);
```

```
I_target2=0.01+0.99*((I_semi_target2-
min(I_semi_target2))/(max(I_semi_target2)-min(I_semi_target2)));
E2=sqrt(I_target2);
%%%%%%%%%%%%%%%%%%%%%% get the wavelets %%%%%%%%%%%%%%%%%%%%%%%%%%%%
b_r2=(dct(E2));
b_r2(513:limit2)=0;
b_r_sum2=sum(abs(b_r2));
b2=round(b_r2/(b_r_sum2/1000))*(b_r_sum2/1000);
E_rec2=(idct(b2));
I_rec2=E_rec2.^2;
I_max2=max(I_rec2);
I_rec_2=I_rec2/I_max2;
%%%%%%%%%%%%%%%%%%%%%% generate target spectrum %%%%%%%%%%%%%%%%%%%%%%
angle=cos((15/180)*pi);
limit3=round((1e12*(2*angle*(5e-6/2^9)./3e8))^-1);
freq=1:limit3;
I_semi_target3=10*exp(-(freq-1990).^2/2000)+3*exp(-(freq-
1950).^2/100)+4*exp(-abs(freq-1910)./300)-3*exp(-abs(freq-
1900).^2/800);
I_target3=0.01+0.99*((I_semi_target3-
min(I_semi_target3))/(max(I_semi_target3)-min(I_semi_target3)));
E3=sqrt(I_target3);
%%%%%%%%%%%%%%%%%%%%%% get the wavelets %%%%%%%%%%%%%%%%%%%%%%%%%%%%
b_r3=(dct(E3));
b_r3(513:limit3)=0;
b_r_sum3=sum(abs(b_r3));
b3=round(b_r3/(b_r_sum3/1600))*(b_r_sum3/1600);
E_rec3=(idct(b3));
I_rec3=E_rec3.^2;
I_max3=max(I_rec3);
I_rec_3=I_rec3/I_max3;
```

```
%%%%%%%%%%%%%%%%%%%%%%%%%%%%%%%%%%%%%%%%%%%%%%%%%%%%%%%%%%%%%%%%%%%%%%%%%%%%
ii=1875:2000;
figure;semilogy(3e6./ii,I_target1(ii),'k',3e6./ii,I_rec_1(ii),'k-
.',3e6./ii,I_rec_2(ii),'k--',3e6./ii,I_rec_3(ii),'k:');
axis([1.5e3 1.6e3 0.7e-1 1]);
xlabel('wavelength (nm)');ylabel('attenuation');title('Spectrum VS
Number of Mirror (10 bits, 2*5um phase range)');
legend('target','2*400','2*1000','2*1600');
%save eugene_final1.mat
```

Appendix D Matlab Program for Gaussian Incident Beam

```
clear all;
%%%%%%%%%%%%%%%%%%%%%% generate target spectrum %%%%%%%%%%%%%%%%%%%%%%
angle=cos((15/180)*pi);
limit1=round((1e12*(2*angle*(5e-6/2^9)./3e8))^-1);
freq=1:limit1;
I_semi_target1=10*exp(-(freq-1990).^2/2000)+3*exp(-(freq-
1950).^2/100)+4*exp(-abs(freq-1910)./300)-3*exp(-abs(freq-
1900).^2/800);
I_target1=0.01+0.99*((I_semi_target1-
min(I_semi_target1))/(max(I_semi_target1)-min(I_semi_target1)));
E1=sqrt(I_target1);
%% reconstruct I(w) with 10bits, 3200 mirrors and 10um phase range %%%
b_r1=(dct(E1));
b_r1(513:limit1)=0;
b_r_sum1=sum(abs(b_r1));
b1=round(b_r1/(0.000625*b_r_sum1))*(0.000625*b_r_sum1);
E_rec1=(idct(b1));
I_rec1=E_rec1.^2;
I_max1=max(I_rec1);
I_rec_1=I_rec1/I_max1;
%%%%%%%%%%%%%%%%%%%%%% generate target spectrum %%%%%%%%%%%%%%%%%%%%%%
angle=cos((15/180)*pi);
limit2=round((1e12*(2*angle*(5e-6/2^9)./3e8))^-1);
freq=1:limit2;
I_semi_target2=10*exp(-(freq-1990).^2/2000)+3*exp(-(freq-
1950).^2/100)+4*exp(-abs(freq-1910)./300)-3*exp(-abs(freq-
1900).^2/800);
I_target2=0.01+0.99*((I_semi_target2-
min(I_semi_target2))/(max(I_semi_target2)-min(I_semi_target2)));
```

```
E2=sqrt(I_target2);
%%%%%%%%%%%%%%%%%%%%%%%%%%%% W=r %%%%%%%%%%%%%%%%%%%%%%%%%%%%%%%%
b_r2=(dct(E2));
b_r2(513:limit2)=0;
b_r_sum2=sum(abs(b_r2));
len2=1:length(b_r2);
modulator2=exp(-((len2-length(b_r2)).^2/(length(b_r2)/2)^2));
b2=round(b_r2/(0.000625*b_r_sum2))*(0.000625*b_r_sum2).*modulator2;
E_rec2=(idct(b2));
I_rec2=E_rec2.^2;
I_max2=max(I_rec2);
I_rec_2=I_rec2/I_max2;
%%%%%%%%%%%%%%%%%%%%%% generate target spectrum %%%%%%%%%%%%%%%%%%%%
angle=cos((15/180)*pi);
limit3=round((1e12*(2*angle*(5e-6/2^9)./3e8))^-1);
freq=1:limit3;
I_semi_target3=10*exp(-(freq-1990).^2/2000)+3*exp(-(freq-
1950).^2/100)+4*exp(-abs(freq-1910)./300)-3*exp(-abs(freq-
1900).^2/800);
I_target3=0.01+0.99*((I_semi_target3-
min(I_semi_target3))/(max(I_semi_target3)-min(I_semi_target3)));
E3=sqrt(I_target3);
%%%%%%%%%%%%%%%%%%%%%%%%%%%% W=r/2 %%%%%%%%%%%%%%%%%%%%%%%%%%%%%%%%
b_r3=(dct(E3));
b_r3(513:limit3)=0;
b_r_sum3=sum(abs(b_r3));
len3=1:length(b_r3);
modulator3=exp(-((len3-length(b_r3)).^2/(length(b_r3)/4)^2));
b3=round(b_r3/(0.000625*b_r_sum3))*(0.000625*b_r_sum3).*modulator3;
E_rec3=(idct(b3));
I_rec3=E_rec3.^2;
```

```
I_max3=max(I_rec3);
I_rec_3=I_rec3/I_max3;
%%%%%%%%%%%%%%%%%%%%%%%%%%%%%%%%%%%%%%%%%%%%%%%%%%%%%%%%%%%%%%%%%%%%%%%%%%%%
ii=1875:2000;
figure;semilogy(3e6./ii,I_target1(ii),'k',3e6./ii,I_rec_1(ii),'k-
.',3e6./ii,I_rec_2(ii),'k--',3e6./ii,I_rec_3(ii),'k:');
axis([1.5e3 1.6e3 0.7e-1 1]);
xlabel('wavelength (nm)');ylabel('attenuation');title('Spectrum VS
Gaussian Beam (10 bits, 2*1600 units, 2*5um phase range)');
legend('target','Planewave','Gaussian Beam, W=r','Gaussian Beam,
W=r/2');
```

Vita

Zhengyu Huang was born in Shanghai, China. He got his Optical Engineering B.S. degree from Tsinghua University in 1999. After graduation, he worked in Lab of Optical Information Processing in the Department of Presition Instruments in Tsinghua University for one year. In 2000 fall, He joined Center for Photonics Technologies of Virginia Polytechnic Institute and State University towards M.S. degree in Electric al Engineering. He is currently interested in DWDM passive devices and fiber optical sensors.